THE UNIVERSITY OF ALBERTA

NANOSECOND BEAM BURST PRODUCTION

A THESIS
SUBMITTED TO THE FACULTY OF GRADUATE STUDIES
IN PARTIAL FULFILMENT OF THE REQUIREMENTS FOR THE DEGREE
OF MASTER OF SCIENCE

DEPARTMENT OF PHYSICS

by

LORNE EDWIN CARLSON

EDMONTON, ALBERTA

SEPTEMBER, 1963

UNIVERSITY OF ALBERTA

FACULTY OF GRADUATE STUDIES

The undersigned certify that they have read, and recommend to the Faculty of Graduate Studies for acceptance, a thesis entitled NANOSECOND BEAM BURST PRODUCTION, submitted by Lorne Edwin Carlson in partial fulfilment of the requirements for the degree of Master of Science.

ABSTRACT

The 5.5 Mev Van de Graaff accelerator at the University of Alberta presently employs a preacceleration beam chopper which produces 500 μ amp beam bunches of 10 nanoseconds duration. The aim of the present work is to develope a top terminal pulsing device, which produces higher intensity 10 nanosecond pulses, by first pulsing the ion source, producing a beam burst longer than 10 nanoseconds, followed by Klystron bunching of this beam to produce the desired 10 nanosecond beam burst. Experimental results indicate that this system (pulsed ion source and buncher) can be employed to produce intense ion beam bursts of 10 nanosecond duration.

ACKNOWLEDGEMENTS

I should like to acknowledge the assistance of the following people.

First, the Professors of the Nuclear Research Centre Group: Drs. G. C. Neilson, W. K. Dawson and J. T. Sample. I should particularly like to thank my Supervisor, Dr. W. K. Dawson, for help with experimental techniques.

Second, the Technicians: L. Holm and E. Cairns for our discussions on electronics; C. Green for his assistance with the construction of the equipment; and J. B. Elliott for his many helpful suggestions on the design of the system.

Also, I should like to thank G. Wait, who worked with me on this project.

Financial assistance from the National Research Council of Canada, in the form of a summer supplement and a bursary, is much appreciated.

TABLE OF CONTENT

LIST OF FIGURES

CHAPTER I. NEUTRON PHYSICS TECHNIQUES

A. Introduction

The nanosecond beam burst production to be described is to be used in conjunction with the University of Alberta's new 5.5 Mev Van de Graaff accelerator. Various types of neutron experiments such as the A(d,n)B and A(n,n')B reactions will be studied with this new accelerator. The need for a pulsed beam from the accelerator comes from the prominence of time-of-flight energy measurement techniques for neutrons and the need for high instantaneous beam current pulses incident on the target. The new 5.5 Mev Van de Graaff at the University of Alberta has a beam chopping device which produces a 10 nanosecond ion beam pulse. The high energy particles are further compressed from 10 nanoseconds to 1 nanosecond by a Mobley Compression Magnet system. The beam chopper and Mobley Magnet will be discussed later in this chapter. The Mobley system compresses a 10 nanosecond, 500 microamp beam pulse into a 1 nanosecond, 5 milliamp beam pulse incident on the target. The work described in this thesis was carried out in an attempt to produce more intense ion beam bursts of 10 nanosecond time duration.

Before these considerations are studied a review of several methods of neutron energy determination will be undertaken.

B. Neutron Energy Determination

The methods used are:

1. Recoil Reactions
2. Neutron Induced Reactions
3. Time-of-Flight

1. Recoil Reactions

(a) Introduction

For neutron energies less than 14 Mev the n-p scattering cross-section is isotropic in the centre of mass system so the proton (knock-on particle) energy spectrum is rectangular, having E maximum proton = E neutron. Above 14 Mev double scattering effects become appreciable and the isotropic effect diminishes, distorting the spectrum.

Hydrogeneous phosphors are used to supply the knock-on particles in most scintillators. However, in gas proportional counters other particles such as deuterons (Ad 53, Tu 53, Al 55) and the elements He (Ba 40), nitrogen and neon (Fo 55), in addition to protons, are used as a supply of knock-on particles.

(b) Experimental Methods

(i) Photographic Plates or Emulsions

The main advantages of this method are: (1) A permanent record of the range, angle and ionization is obtained. This gives a greater discrimination against background from scattered neutrons, electrons, and gamma rays. Resolutions obtained here are as good as those obtained by other methods in the 1 to 20 Mev range. (2) The experimental setup is simple. (3) It is economical in accelerator running time, and having no elaborate electronics, it is inexpensive. (4) It is physically small so may be placed inside reactors with no great perturbing effects on the neutron density. Its continuous sensitivity and lightness make it suitable for high altitude balloon work.

The main disadvantage of this method comes from the long periods of scanning the emulsion and calculations needed to obtain results.

Two main experimental methods are used in working with photographic emulsions as neutron detectors:
(1) In the first method an hydrogeneous radiator external to the detecting emulsion is used to produce the knock-on particles. (2) In the second method the emulsion acts as the source of knock-on particles as well as the detector.

(1) The External Radiator

This method is used when working with high neutron fluxes. It is the more accurate of the two methods. The radiator is an hydrogeneous target. An emulsion detector at an angle ψ_p to the incident neutron beam detects protons knocked from the radiator. Protons enter the detector at an angle ψ_b to the detector surface. The proton range is thus given by

$$R_t = R_h \sec \psi_b$$

where R_t is the true range, R_h is the surface range. The neutron energy is

$$E_n = E_p \sec^2 \psi_p$$

where E_n is the neutron energy, E_p the proton energy from range energy relations, and ψ_b is the average proton angle to the emulsion with respect to the neutron beam.

The energy range is from 0.9 Mev to hundreds of Mev governed mainly by the proton range in the detector and the detector thickness.

2. The Internal Radiator

The emulsion acts as both the radiator and detector

in this method. The detector's surface is at an angle ϕ to the neutron beam. This method has the advantage of simplicity over the above method. Energies down to 0.2 Mev may be measured, governed by a minimum range of about 3 microns for track identification. The previous method had a loss of several hundred kev in the radiator. At the same energy resolution a flux measurement 1/20 that for an external radiator may be made. The maximum energy measurable is about 25 Mev due to coulomb scattering of the protons. The measurement task is made easier if only those tracks within a cone of 15° to the incident direction are measured, so the true and surface ranges are approximately equal.

(ii) Cloud Chambers

The cloud chamber was the first major neutron detector. It is well adapted to the detection of neutrons using the proton recoil method in that the range of the recoil path and its direction in space are recorded. The cloud chamber has a low duty cycle suited to pulsed sources. It is mainly used in the 0.1 to 1 Mev energy range. Modern cloud chamber techniques are discussed in the reference (St 60). The simplicity and speed of modern nuclear emulsion recording has supplanted the use of the rather bulky and cumbersome cloud chamber.

The Diffusion Cloud Chamber, a continuously sensitive one, has been developed to the stage of research quality (Sn 53). Recently the Bubble Chamber (Gl 52) has been developed. A complete discussion is given by Glaser (Gl 56). It is used in the very high energy range (Ce 56).

(iii) Gas Recoil Detectors

For a proportional counter with an amplification factor greater than 10 the measured energy of the detected particle is independent of the initial position of ionization in the counter. If a geometric limitation permits detection of only those particles projected in a forward direction, the resulting energy spectrum will be a faithful replica of the incident neutron spectrum, $E_p = E_n \cos^2\phi \approx E_n$.

The useful energy range is 20 kev to 3 Mev (Fe 60). Double scattering sets the upper neutron energy. The gas amplification factor should be between 10 and 30, the upper limit being set by gamma ray background. Scattered neutrons also enhance the background.

Energy resolutions of 10% with an efficiency in the order of 10^{-4} have been obtained (Gi 50, Gi 53). Gamma ray insensitive detectors have been employed (Pe 56) with however a further lowering of the neutron detection efficiency.

This method is not generally used as it demands too complicated an experimental arrangement compared to other methods (4), and is less versatile than time-of-flight techniques.

(iv) Scintillators

Scintillators containing hydrogen can be used to detect fast neutrons (Sw 60) as the neutrons produce recoil protons in the scintillator itself. This type of scintillator is similar in many ways to a gas recoil counter operating with a gas of high density.

In practice, organic scintillators containing only carbon and hydrogen (anthracene, stilbene, various plastics, and various liquids) offer the most convenient means of obtaining a high proton concentration.

Several methods are used to distinguish between the neutron flux and background effects. They are: (1) Pulse shape discriminators distinguish between charged particle pulses and gamma ray induced pulses due to their different ionization properties. (2) The size and geometrical shape of the scintillator may be chosen to minimize the number of counts due to electrons. (3) Several scintillators may be used in coincidence.

2. Neutron Induced Reactions

(a) Introduction

Neutron induced reactions such as $n + A \rightarrow B + C + Q$ may be used to obtain a neutron pulse height spectrum. For the low energy spectrum the value of Q must be positive. Because the energy resolution of this type of system increases with decreasing Q, a low Q reaction should be used for the low neutron energy spectrum determination. He^3 is the main isotope used in this type of detector (Ba 60). Alternately using various negative Q reactions the neutron energy may be roughly related to the thresholds of these reactions. A discussion of various fission threshold detectors by R. W. Lamphere is found in reference (La 60). The threshold detector has the advantage of counting only those neutrons whose energy is above the threshold energy, thus reducing the low energy background. They are used in reactors to measure the fast flux, and in recording fast flux occurring in sudden bursts as with nuclear explosions.

A few of the principal neutron detection reactions are listed below. They are termed thermal neutron reactions since the reaction cross-section is largest for low energy neutrons.

Absorption (n,α)

$$n + B^{10} \rightarrow Li^{7*} + He^{4} + 2.3 \text{ Mev}$$

$$Li^{7*} \rightarrow Li^{7} + \gamma(480 \text{ kev})$$

$$n + Li^{6} \rightarrow He^{4} + H^{3} + 4.64 \text{ Mev}$$

Fission (n,f)

$$n + U^{235} \rightarrow X + Y + \nu n + 200 \text{ Mev}$$

(b) Experimental Methods

(i) Solid State Detectors

For charged particles the surface barrier solid state detectors show a wider dynamic range and a characteristically smaller low energy background than do scintillation counters. The solid state detector is, however, relatively insensitive to neutron and gamma radiation. (Br 62) Extensive efforts are now being devoted to adopting the detectors for these radiations.

This type of detector has been used with thermal neutrons. Semiconductors were coated with fissile materials (Da 61, NRE 61) such as U^{235}. Other coatings lead to the solid state detectors use with the reactions:

$$He^{3}\ (n,p)\ H^{3}$$

Li^6 (n,α) T

B^{10} (n,α) Li^7

A type of semiconductor detector which is possible but has not yet been reported is the threshold detector foil on a solid state detector. An example is the C^{12} converter plus detector system. It does not respond for En < 5.8 Mev where the n,γ reaction becomes energetically possible. No other charged particles are produced for En < 13.6 Mev where the n,p process becomes possible.

(ii) Scintillators

Scintillation media may be either gaseous, liquid, or solid. The Li^6 reaction is often used for neutron detection with scintillators. The initiating nuclear reactions generate single or multiple energy pulses in the solvent or host medium. This energy is either radiated or it is transformed by a radiationless process to luminescent centres. The luminescent centres radiate light which is detected either directly or after having been absorbed and reradiated by a wavelength shifting material. The time involved for these processes depends on the chemical and physical nature of the phosphor. Solid inorganic phosphors display decay times $\gtrsim$ 1 microsecond, while noble gases and organic phosphors exhibit decay times $\gtrsim$ 1 nanosecond.

(iii) Gas Counters

Gas counters have been used to detect the presence of neutrons since the 1940's. The most utilized gas counter is the $B^{10}F_3$ gas counter based on the reaction:

$$n + B^{10} \rightarrow Li^{7*} + He^{4} + 2.3 \text{ Mev}$$

$$Li^{7*} \rightarrow Li^{7} + \gamma(480 \text{ kev})$$

However, it is necessary to moderate the incident neutrons to thermal energies. This moderation is usually accomplished using paraffin or graphite moderating shields.

This method of neutron detection lends itself to flux measurements rather than to energy measurements.

3. Time-of-Flight Techniques

(a) Introduction

A good review of the basic techniques used in neutron spectrometry is Suffield Technical Paper No. 176 by G. C. Neilson *et al* (Ne 60). The following section gives a brief outline of the corresponding sections of that paper.

The development of nanosecond pulse circuitry, fast phosphors and high gain, low noise photomultipliers has led to a wide use of time-of-flight techniques for precise neutron energy determination. Interest in fast neutron spectroscopy and inelastic scattering cross-sections

stimulated the rapid advance in the techniques to the nanosecond region. The following discussion will be limited to the neutron energies less than 10 Mev, the energy region now under study at this University. A 1 Mev neutron takes approximately 70 nanoseconds to traverse a one meter flight path.

To measure the neutron's energy, a zero time, i.e. the time at which the neutron begins its flight and the flight time or time elapsed from zero time until the neutron is detected at the end of its flight path, are needed. This leads to two related problems, each solvable in a number of ways.

(b) Methods of Obtaining a Zero Time

There are three basic methods used to obtain the zero time. They are:

- (i) Associated Particle
- (ii) Secondary Particle or Gamma Ray
- (iii) Pulsed Beam

(i) Associated Particle

In this method the second or recoil particle emitted in the nuclear reaction is detected very near to its point of origin. The detection of this particle in coincidence with the neutron greatly reduces the background.

In many nuclear reactions (including inelastic neutron scattering) the product nucleus is left in an excited state. The gamma ray emitted by these nuclei usually have a life time which is short compared to the time resolution of the spectrometer employed and they may be used to indicate the zero time. The associated gamma ray is easier to detect than the associated particle because the gamma detector unlike that of the associated particle need not be contained in the target chamber. The use of solid state detectors reduces the space problems formerly encountered.

(ii) Secondary Particle or Gamma Ray

An indication of zero-time can also be obtained at the expense of a small amount of energy from the neutron as it begins its flight or by taking a relatively large amount of energy and so changing the energy of the neutron by a calculable amount. Thus, as an example of the first method, Fraser and Milton (Fr 58) detected the secondary electrons or delta-rays ejected from a thin foil near the source by a fission fragment passing through it. The fragment lost about 500 kev of energy in the foil and continued along its flight path with very nearly its full energy. The second method is more applicable to

lighter particles and has been used successfully with neutrons. Neilson and James (Ne 55) scattered neutrons through an angle θ from a stilbene crystal and detected them in coincidence in a second crystal some distance away. Sufficient energy, $E_o \sin^2\theta$ was given to the proton recoil in the first crystal to produce a zero-time output pulse from the photomultiplier, and the energy of the scattered neutron detected in the second counter was given by $E_n = E_o \cos^2\theta$ where E_o was the original neutron energy. They measured E_n by time-of-flight between the two counters, and, with a knowledge of θ, could calculate E_o. In both cases fairly well defined beams of mono-energetic neutrons could be obtained for further experiments.

(iii) Pulsed Beam

The pulsed beam may be applied to all types of reactions. It gives a zero time independent of the reaction mechanism. In this method the beam of incident particles which initiates the reaction is pulsed onto the target for a time period much shorter than the neutron flight time to be measured, and at such a repetition rate that the longest flight time of interest may be measured before the next pulse reaches the target.

There are two main methods of pulsing a steady beam source. They are:

1. Pulsing the ion source
2. Chopping the beam

There are two further methods used to decrease the duration of pulses formed by the above methods:

3. Klystron bunching
4. Variable path length (Mobley Magnet)

These four pulsing methods will be examined in the next section.

(c) Measurement of Time-of-Flight

The first systems used (Ja 51) determined the coincident count rate between the initial and final pulses as a function of inserted time delay. These systems had insufficient time resolution needing faster coincidence circuits, and poor efficiency.

Lefevre and Russell (Le 59) developed a type of chronotron, a multichannel time delayed coincidence analyser, called a vernier chronotron. Two delay cables are used with the system rather than the single delay cable of former systems. Both delay cables are formed into circles. The initial and final pulses are fed into

their respective delay cables. The time delay of the terminal pulse line is made slightly shorter than the time delay of the initial pulse line. As the two pulses travel around their circular paths the time interval between the two pulses diminishes. The pulses circulate until a time coincidence between them is detected. If the lines differ in length by 1 nanosecond a count of the number of transits before coincidence gives the original time difference directly in nanoseconds. This number thus indicates the channel in which one count is to be stored and is a presentation suited for use with the magnetic storage system of various commercial pulse height analysers.

A different approach to the problem of measuring the time interval between two pulses originated from the proposal of Moody (Mo 52) of converting the time spectrum into a pulse height spectrum. In this method the time interval between two fast pulses is converted into a slow pulse whose height is proportional to the interval. Using this principle several workers (Ne 55, Re 57, Gr 58, Le 55, Jo 56, We 56) have developed practical "time converters" for use in the nanosecond region.

C. Methods of Obtaining Nanosecond Beam Bursts

As stated in the previous chapter there are two methods

used to produce an ion beam burst. The first consists of pulsing the ions out of the ion source itself, while the second takes a steady beam of ions from the ion source and chops the beam into small sections. It is possible to obtain 1 nanosecond pulses using either of these methods alone, but the beam burst intensity will be very low. To increase the beam burst intensity the above methods are used to produce pulses longer than the desired 1 nanosecond, say 10 nanoseconds. These pulses are further compressed to 1 nanosecond using either a Klystron buncher or Mobley compression magnet. The instantaneous current at the target is increased markedly now as the current corresponds to a 10 nanosecond burst rather than a 1 nanosecond burst.

1. Ion Source Pulsing

Plasma pulsing is one means of obtaining a bunched beam. In this method the ion source itself is pulsed, whereas in the next method the ion source is run under steady state conditions. The plasma pulsing method is the most efficient one for beam burst production in that a greater number of the ions leaving the ion source reach the target as compared with other methods. It has less beam degradation than do chopping or bunching. The

problems here are the control and utilization of the applied modulation.

2. Beam Chopping

One of the more used methods of ion beam pulsing is the post acceleration beam flipper, as employed in the University of Alberta's Nuclear Research Centre 2.0 Mev Van de Graaff accelerator. While this chopping method produces bursts in the nanosecond range leading to small experimental errors in the neutron energy calculation, it does, however, have a very low efficiency in that approximately 99% of the ion beam must be deflected and lost to the experimentor to obtain the 1 nanosecond beam pulses.

Figure 1 shows a simple system used to sweep a beam past a slit thus producing short bursts from a steady beam. A sinusoidal radio frequency voltage across the plates sweeps the beam across the slits S. By appropriate choice of the system parameters nanosecond pulses may be formed, and allowed to impinge on the target. The zero time may thus be timed relative to the phase of the deflecting voltage or relative to the beam current pulse on the target.

This method of beam burst production has two basic

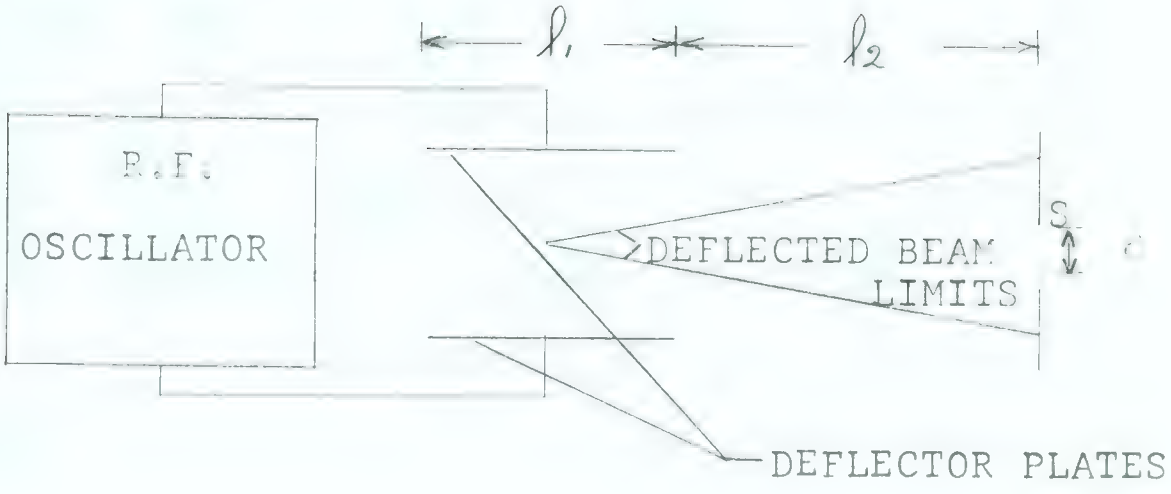

FIGURE 1. SIMPLE BEAM CHOPPER

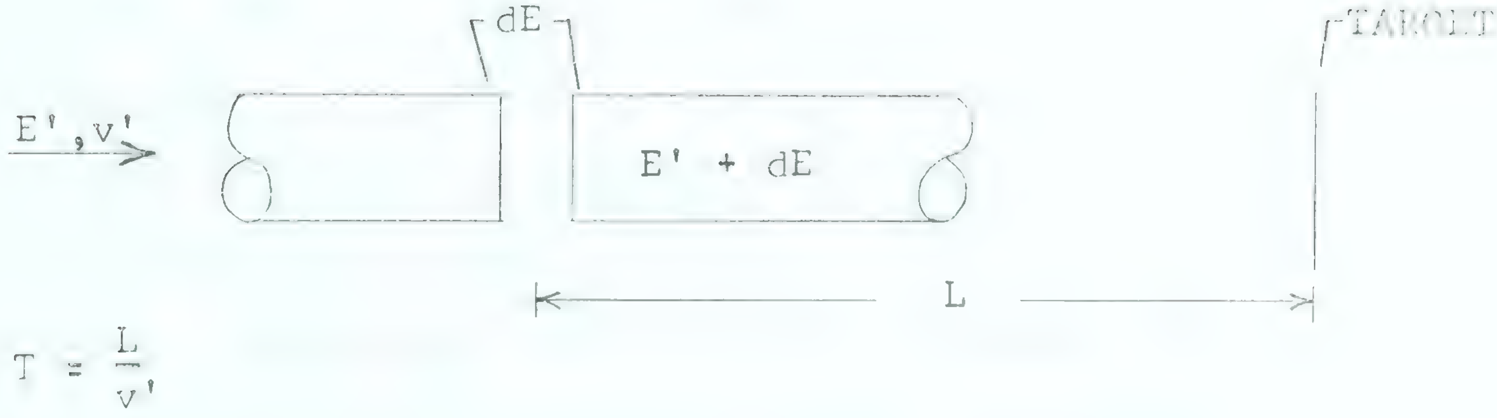

FIGURE 2. SIMPLE KLYSTRON SINGLE TUBE BUNCHER

weak points. Firstly, as stated above, the efficiency of utilization of the steady ion beam is small. The minimum usable pulse duration is determined by the intensity of the steady beam, the efficiency of the detection system, and the reaction under study. Secondly, the large percentage of the beam not traversing the slits may lead to a high background radiation, a serious problem when neutron experiments must be done in cramped quarters.

C. M. Turner (Tu 58) some years ago proposed a simple method to overcome the above difficulties, namely preacceleration chopping. The "chopper" is introduced between the ion source and the high voltage terminal of the electrostatic accelerator. A series of short bursts rather than a steady beam is accelerated so the above mentioned background effects are overcome. Also, as it has been shown that an electrostatic accelerator is sensitive to the average rather than the instantaneous current in the beam, the pulse intensity may be raised as long as the pulse time duration is short compared to the ionization loading time constant which is of the order of a few milliseconds (Tu 49).

The main disadvantage arising from the chopper being at a high potential end of the Van de Graaff accelerator is the lack of adequate space to obtain a suitable lever

arm for the chopper. However, as the beam energy is still low the lever arm is smaller than would be needed for post acceleration chopping. This problem does not exist in the small (150 kv) accelerator constructed by the author as the negative power supply permits the ion source to be at ground potential. Preacceleration chopping has been carried out successfully by groups at Oak Ridge National Laboratories (Ne 56) and the University of California (Bl 56).

A more detailed treatment of beam chopping is found in the following chapter.

3. Klystron Bunching

An ion beam burst, produced by either of methods 1 or 2 above, consists of a series of ions travelling along an axis and having a definite spacing between the extreme ions. The beam pulse duration is given by the time taken for all of these ions to pass a point on the axis. It is possible to decrease the length of the beam burst, thus the beam pulse duration, by correctly changing the energy of each ion. The energy increment is imparted to each ion as the ion passes a definite position along the axis (acceleration gap). It is proportional to the time interval between the arrival, at the acceleration gap, of

that ion and the first ion of the beam burst. This decrease in pulse time spread or increased instantaneous current is gained at the expense of an energy spread in the beam; the energy of the last ions of the beam bunch was increased.

Simple klystron bunching, applying a sinusoidal voltage across a small gap, is one method of doing this. The ions traversing the gap near the zero phase of the modulating voltage will be further bunched, an amount depending upon the physical factors of the system. A mathematical treatment will be found in the following chapter. The main difficulties of simple klystron bunching are that the bunching can occur only over a short period of the modulating voltage, and the energy dispersion of the beam is increased by

$$dE_1 \cdot dt_1 = dE_2 \cdot dt_2$$

where dE is the beam energy spread, dt is the beam time spread, and the subscripts 1 and 2 refer respectively to the periods before and after the beam is bunched.

Delenay (De 55) has proposed the equation

$$dE = E' \left((1 - t/T)^{-2} - 1 \right)$$

for perfect bunching from a single bunching tube. Here a larger acceptance phase is involved. T is the unmodulated

flight time, t is the prebunching pulse length, E' is the initial beam energy, and dE is the applied modulating voltage. Space charge effects have been neglected.

4. Variable Path Length (Mobley Compression Magnet)

A further method of shortening a pulse is to make the distance travelled to the target by the first ions of the pulse greater than the distance travelled by the last ions of the pulse. This method, generally known as the Mobley (Mo 52) magnet buncher employs, as the name suggests, a magnet whose stationary magnetic field is so devised and the beam swept across it in such a manner that the rays passing through it in sequence arrive at the same instant at some target point on which all such rays converge to a focus.

The details of such a system are found in the next chapter. The magnet may be a double focussing one, with deflector plates at one focus and the target at the other focus. This method produces a pulse on the target of time spread proportional to the beam width, H, at the deflector plates and inversely proportional to the beam sweep velocity, v', across the magnet. It has the advantage that it reduces the problem of space-charge repulsion, and unlike the Klystron method, it adds little

to the beam energy spread. On the other hand, the equipment is very expensive and bulky, and great care must be taken to sweep the beam at a linear rate across the magnet to ensure perfect time coincidence at the target. A change in beam energy necessitates a change in sweep voltage and magnetic field intensity to refocus the beam on the target; this may be carried out automatically through the use of beam sensing (sniffer) plates and feedback circuits. The expense of obtaining a shortened beam bunch is an angular spread introduced into the beam by the magnet. It is usually desirable to keep this spread under 1°. The increased instantaneous current on the target usually offsets the small angular spread obtained. Figure 3 is a line diagram of a Mobley magnet system.

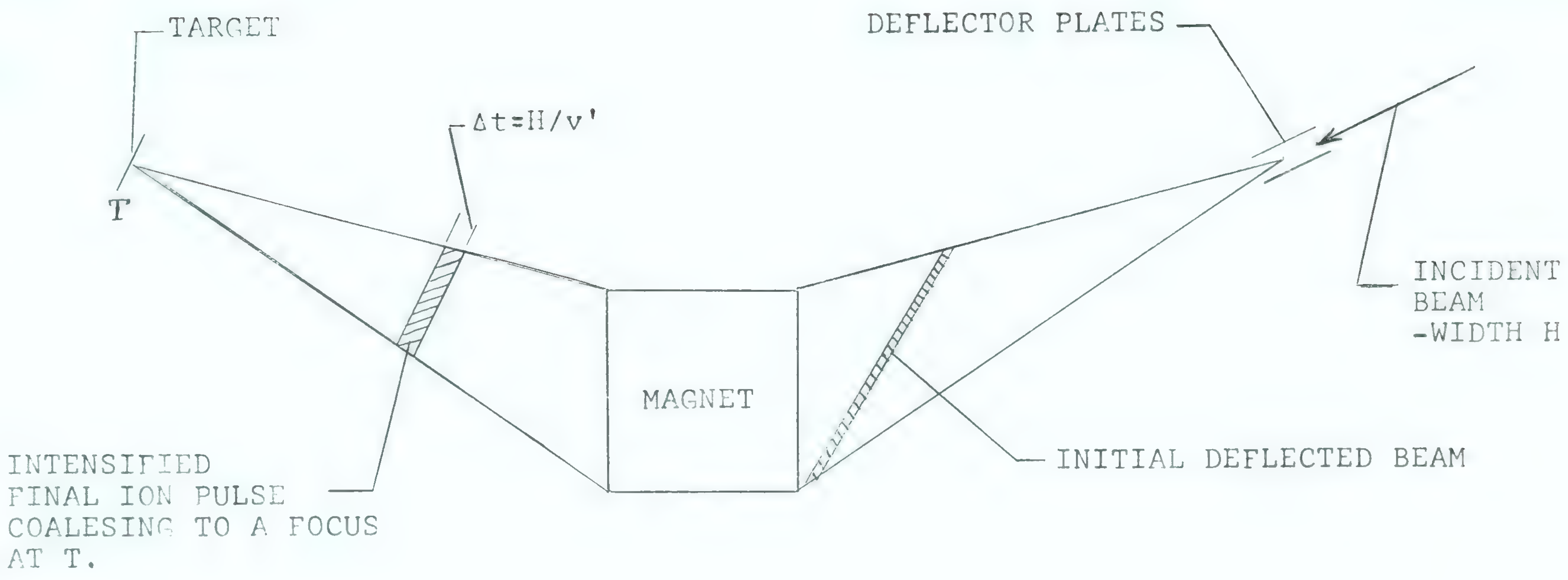

FIGURE 3. MOBLEY MAGNET SYSTEM

CHAPTER II. THE MATHEMATICS OF BEAM BUNCHING

A. Introduction

This chapter will deal with the mathematics of nanosecond beam burst production. It starts off with a simple treatment of beam chopping, followed by a more rigorous treatment of a monoenergetic axial beam. Effects of finite sized beams and beam energy spread are then discussed. A further discussion of Klystron bunching and the Mobley magnet system round out the chapter.

An ion can emerge from the sweeping plates with zero angular deviation only if it arrives at the centre of the plates at 0 or π phase, thus receiving equal and opposite transverse momentum impulses during its time in each half of the plates. Although this beam will have zero angular deviation, the beam will be displaced off axis. Figure 4 shows the trajectory of an axial ray which emerges with zero angular deviation. Consider the beam burst accepted at a time when the r.f. voltages are such that the top plate is slightly positive in voltage, the bottom plate slightly negative, and both these voltages are going towards zero. The positive ion thus sees a negative potential gradient towards the lower plate and the ions

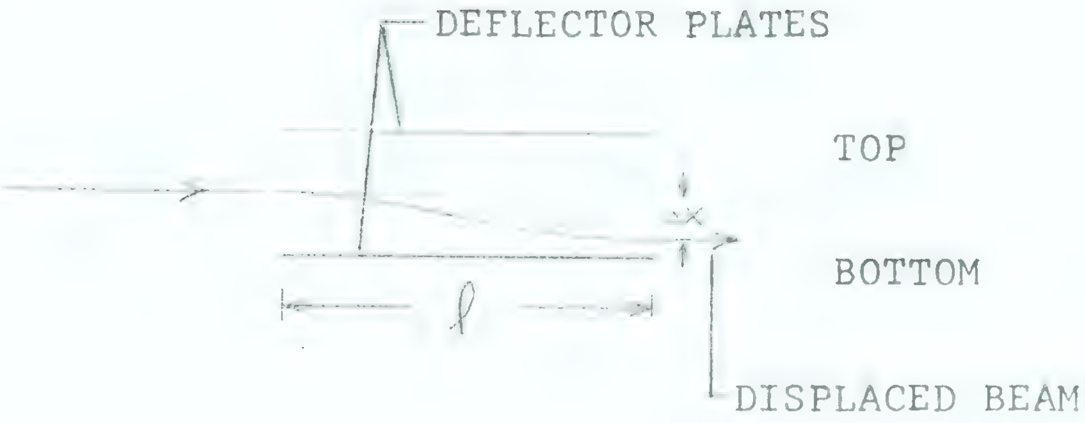

FIGURE 4A. TRAJECTORY OF BEAM BURST WHICH ENTERS THE DEFLECTOR PLATES SO THAT IT REACHES THE VERTICAL PLATE CENTRE AT ZERO r.f. VOLTAGE PHASE.

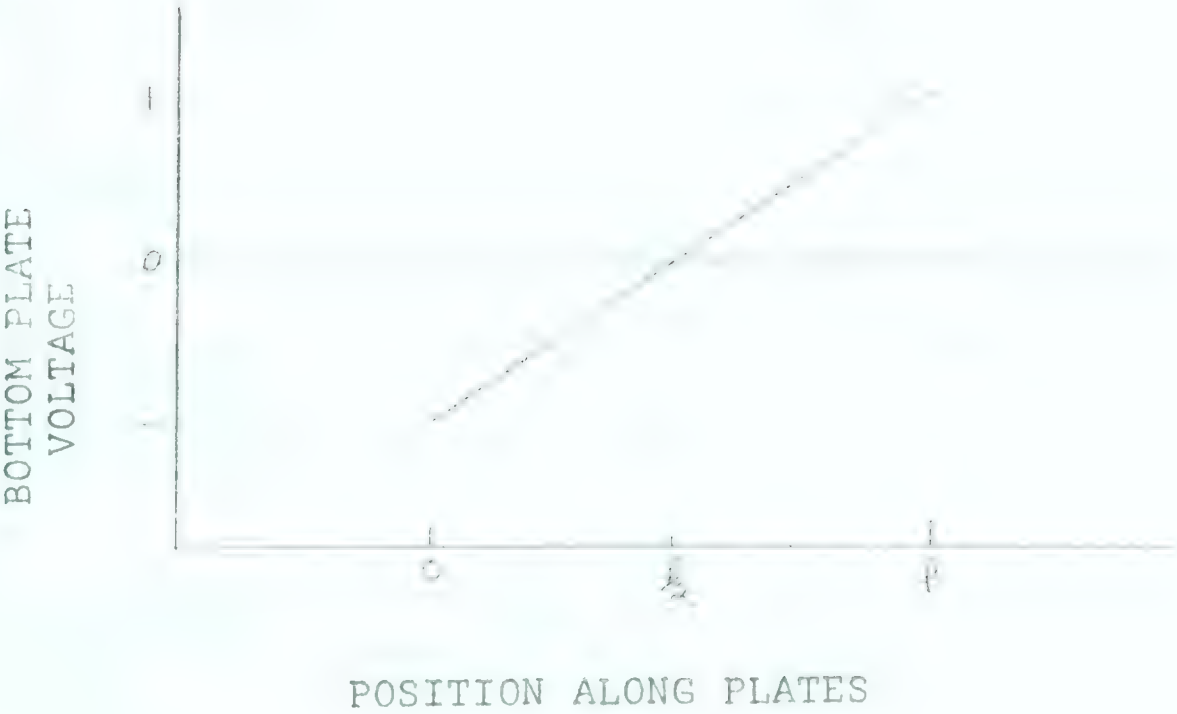

FIGURE 4B. VOLTAGE ON BOTTOM DEFLECTOR PLATE VERSUS HORIZONTAL POSITIVE ION POSITION BETWEEN PLATES

are forced towards this lower plate. When the ion has travelled half the distance along the length of the plates both upper and lower plates have zero potential and no force exists on the ion, but the ion does have a downward velocity component. Past this centre the voltages have reversed. The top plate is now negative and the bottom plate positive. The ion experiences a force towards the top plate until at the edge of the plates the vertical velocity component is zero. The beam exits from the plates with zero angular divergence but is displaced below the horizontal axis. As the last force seen by the positive ion was upwards, this beam burst is termed the upsweep.

Similarly, the beam burst, which is accepted when the r.f. voltage phase has advanced π radians from the acceptance of the upsweep beam burst, is moved above axis, again with zero angular deviation. This beam burst is known as the downsweep.

The magnitude of the lateral displacement of the beam during each sweep is given by C. M. Turner and S. D. Bloom (Tu 58) to first order, by

$$\Delta X = (E' \omega l_1^3)/(16 V v)$$

where E' is the peak r.f. voltage applied to the deflecting

plates, ω is $2\pi f$, l_1, is the plate length, V is the pre-acceleration potential difference, $eV = 1/2\ mv^2$, and v is the ion velocity.

It is desirable to suppress one of these sweeps completely to realise the advantage of optimum transmission efficiency for the other sweep.

Also as the detector can pick up only one signal per r.f. cycle, giving a zero time for one of the pulses, the second pulse is background. This is done using a set of refractor plates cross connected to an adjustable d.c. power supply. By proper adjustment of the d.c. bias one of the beams can be placed on axis while the other is further displaced off axis. Turner and Bloom (Tu 58) suppressed the alternate sweep by a ratio of better than 1000 to 1 with respect to the passed sweep.

Alternately the beam defining slits may be moved off axis, permitting only one of the sweeps to continue to the target

B. Theory of Beam Chopping

1. Elementary Theory of Beam Chopping

Chopping a beam by employing a set of deflector plates with a variable voltage to sweep a beam of positive ions past an aperture constitutes a positive ion oscilloscope

(Ne 60 b). Turner and Bloom (Tu 58) have presented a theory for a positive ion oscilloscope.

An elementary probe into beam chopping will be taken before a more detailed study is undertaken. The following theory follows that found in Fast Neutron Physics by Neiler and Good (Ne 60).

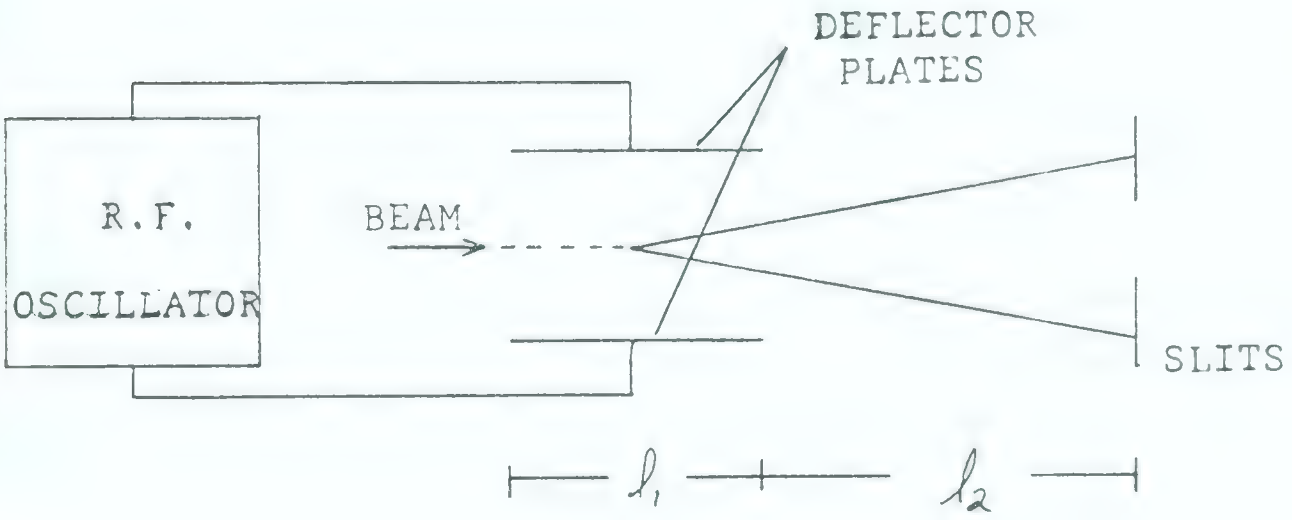

Figure 5. Simple Deflector Plate and Ion Beam Defining Slits

In the following work the fringing effects and space charge effects will be neglected

If the flight time, l_1/v_0, through the deflector plates, Figure 5, is small compared to the period, T, of the

sinusoidally varying voltage, and the particles traverse the acceleration plates near zero phase, the applied voltage may be considered to be a ramp function

$$\mathcal{E}_y = -V/d = -\left(\frac{V_0}{d}\right)\left(\frac{2\pi t}{T} + \delta\right) \tag{1}$$

We assume the beam is initially monoenergetic with $E_0 = \frac{1}{2}mv_0^2$. The phase shift factor δ is given by ωt_0. It represents the difference, from the zero voltage phase, of the voltage phase upon the particles entrance into the plates. We know that the distance off axis at the screen is given by

$$y_{sc} = y(l_1) + \tau_2\, \dot{y}(l_1) \tag{2}$$

τ_2 is considered to be a constant given by $\tau_2 = l_2/v_0$. The variation in y_{sc} with a variation in the entrance phase δ will now be found.

$$m\ddot{y} = \left(\frac{eV_0}{d}\right)(\omega t + \delta) \qquad ; \ \delta \equiv \omega t_0 \tag{3}$$

$$\dot{y} = \left(\frac{eV_0}{md}\right)\left(\frac{\omega t^2}{2} + \delta t + c_1\right)$$

$$y = \left(\frac{eV_0}{md}\right)\left(\frac{\omega t^3}{6} + \frac{\delta t^2}{2} + c_1 t + c_2\right)$$

$$y_{sc} = \left(\frac{eV_0}{md}\right)\left\{\omega\left(\frac{t_1^3}{6}+\frac{\tau_2 t_1^2}{2}\right)+\delta\left(\frac{t_1^2}{2}+\tau_2 t_1\right)+C_1(t_1+\tau_2)+C_2\right. \qquad (4)$$

$$\frac{dy_{sc}}{d\delta} = \left(\frac{eV_0}{md}\right)\left(\frac{t_1^2}{2}+\tau_2 t_1\right)$$

$$\therefore \quad \Delta y_{sc} = \frac{1}{4}\left(\frac{eV_0}{Ed}\right)\left(l_1^2+2l_1 l_2\right)\Delta\delta \qquad (5)$$

We now have

$$\Delta t_0 = 4\left(\frac{Ed}{\omega eV_0}\right)\frac{\Delta y_{sc}}{l_1(l_1+2l_2)} = \frac{\Delta y_{sc}}{\text{W. S.}} \qquad (6)$$

where w.s. is the writing speed = $\{\omega e V_0 l_1(l_1+2l_2)\}/(4Ed)$ It follows that chopping can be carried out whatever the energy, as long as the deflector plate length and distance to the aperture are correspondingly changed.

A preacceleration beam chopper operating under the following conditions would produce a beam burst, beyond the beam defining slits, of 10 nanoseconds time duration:

E(kev)	d(cm)	Δy(cm)	V_0(kev)	ω meg c/s	l_1(cm)	l_2(cm)
4	1.0	0.4	4	2	5	5

2. An Extended Theory of Deflector Plates

(a) The Monoenergetic Axial Ray

The above simple treatment gives a reasonable estimate of the beam burst duration produced by the configuration of Figure 1, to the extent of the axial ray assumption. It does not, however, predict the two images actually observed.

The following theory presents a solution of the axial ray problem which makes no assumptions about the relative values of the phase angles encountered in the problem. In this treatment the assumption of an ion transit time less than the sweep voltage period is not made, rather the transit time may be a considerable fraction of the sweep period. In addition the deflector plates are in two equal sections (Figure 6), permitting independent d.c. biasing indicated by V_{DC_1}, V_{DC_2} respectively. This eliminates the need for an additional refractory plate (see section 2f). The costly top terminal space, which would be taken up by the refractory plate, is thus free for other uses.

Figure 6. Schematic of Split-Deflector-Plate Ion Beam Pulser

When an a.c. voltage $V_{AC} = V_{AC_0} \cdot \sin \omega t$ is applied across both sets of plates, the equations of motion are

$$m\ddot{z} = 0$$

$$m\ddot{y} = \left(\frac{eV_{AC_0}}{d}\right) \sin \omega t + \left(\frac{eV_{DC_1}}{d}\right); \quad 0 < z < \frac{l_1}{2}$$

$$= \left(\frac{eV_{AC_0}}{d}\right) \sin \omega t + \left(\frac{eV_{DC_1}}{d}\right); \quad \frac{l_1}{2} < z < l_1 \qquad (7)$$

The fringing effects will be neglected, and the transit time between deflector plates is considered negligibly small. The particle velocity is considered to remain essentially constant. The transit times are given by $\tau_1 = \frac{l_1}{v_0}$ and $\tau_2 = l_2/v_0$. The distance l_2 will be expressed in terms of l_1 as $l_2 = kl_1$. k is known as the lever arm. Also the length l_1 will be expressed as an angle $\delta_1 = \omega l_1/v_0 = \omega\tau_1$; δ_1 is the plate length in radians.

For an incident axial ray

$$y_{sc} = y(\delta_1, k, \omega t_0, V_{AC_0}, V_{DC_1}, V_{DC_2})$$

$$= y(\delta_1, ---) + \tau_2 \dot{y}(\delta_1, ---) \; ; \; \delta \equiv \omega t \qquad (8)$$

Thus

$$\frac{dy_{sc}}{dt_0} = dy(\delta_1, ---)/dt_0 + \tau_2 \, d\dot{y}(\delta_1, ---)/dt_0$$

Now

$$\dot{y} = \left(\frac{eV_{AC_0}}{md}\right) \sin \delta \quad + \left(\frac{eV_{DC_1}}{md}\right) \qquad 0 < z < \frac{l_1}{2}$$

$$= \left(\frac{eV_{AC_0}}{md}\right) \sin \delta \quad + \left(\frac{eV_{DC_2}}{md}\right) \qquad \frac{l_1}{2} < z < l_1$$

Therefore

$$\dot{y} = \left(\frac{eV_{AC_0}}{md}\right)\left\{\int_{t_0}^{t_{\frac{1}{2}}} \sin\delta \, dt + \left(\frac{V_{DC_1}}{V_{AC_0}}\right)\int_{t_0}^{t_{\frac{1}{2}}} dt\right\}$$

$$+ \left(\frac{eV_{AC_0}}{md}\right)\left\{\int_{t_{\frac{1}{2}}}^{t_1} \sin\delta \, dt + \left(\frac{V_{DC_2}}{V_{AC_0}}\right)\int_{t_{\frac{1}{2}}}^{t_1} dt\right\} \quad ; \; t_{\frac{1}{2}} = t_0 + \frac{l_1}{2v_0}$$

Changing variables from t to δ we have

$$\dot{y} = \left(\frac{eV_{AC_0}}{md\omega}\right)\left\{\int_{\delta_0}^{\delta_0+\delta_1} \sin\delta \, d\delta + \left(\frac{V_{DC_1}}{V_{AC_0}}\right)\int_{\delta_0}^{\delta_0+\frac{\delta_1}{2}} d\delta + \left(\frac{V_{DC_2}}{V_{AC_0}}\right)\int_{\delta_0+\frac{\delta_1}{2}}^{\delta_0+\delta_1} d\delta\right\}$$

giving

$$\dot{y} = \left(\frac{eV_{AC_0}}{md\omega}\right)\left\{\cos \omega t_0 - \cos(\omega t_0 + \delta_1)\right\}$$

$$+ \left(\frac{eV_{AC_0}}{md\omega}\right)\left\{\left(\frac{V_{DC_1}}{V_{AC_0}}\right)\frac{\delta_1}{2} + \left(\frac{V_{DC_2}}{V_{AC_0}}\right)\frac{\delta_1}{2}\right\} \qquad (9)$$

Consider δ as an independent variable with limits δ_0 to $\delta_0 + \delta_1$.

$$y = \left(\frac{eV_{AC_0}}{md\omega}\right)\left\{\int_{\delta_0}^{\delta_0+\delta_1}(\cos\omega t_0 - \cos(\omega t_0+\delta_1))\,d\delta + \left(\frac{V_{DC_1}}{V_{AC_0}}\right)\int_{\delta_0}^{\delta_0+\frac{\delta_1}{2}}\delta\,d\delta + \left(\frac{V_{DC_2}}{V_{AC_0}}\right)\int_{\delta_0+\frac{\delta_1}{2}}^{\delta_0+\delta_1}\delta\,d\delta\right\}$$

i.e.

$$y = \left(\frac{eV_{AC_0}}{md\omega^2}\right)\left\{\sin\omega t_0 - \sin(\omega t_0+\delta_1) + \delta_1\cos\omega t_0\right\}$$

$$+\frac{1}{2}\left(\frac{eV_{AC_0}}{md\omega^2}\right)\left\{\left(\frac{V_{DC_1}}{V_{AC_0}}\right)\left(\frac{\delta_1}{2}\right)^2 + \left(\frac{V_{DC_2}}{V_{AC_0}}\right)\left(\frac{\delta_1}{2}\right)^2\right\} \qquad (10)$$

Neiler had the factor 3 multiplying his V_{DC_1} term. It appears for the limits $-\delta_1$ to 0.

It follows that

$$\begin{aligned} y_{sc} = \left(\frac{eV_{AC_0}}{md\omega^2}\right)\Big\{ & \left[\sin\omega t_0 - \sin(\omega t_0+\delta_1) + \delta_1\cos\omega t_0\right] \\ & + \delta_2\left[\cos\omega t_0 - \cos(\omega t_0+\delta_1)\right] \\ & + \frac{1}{2}\left(\frac{\delta_1}{2}\right)^2\left[\frac{V_{DC_1}}{V_{AC_0}} + \frac{V_{DC_2}}{V_{AC_0}}\right] \qquad (11) \\ & + 2\left(\frac{\delta_2}{2}\right)\left(\frac{\delta_1}{2}\right)\left[\frac{V_{DC_1}}{V_{AC_0}} + \frac{V_{DC_2}}{V_{AC_0}}\right] \end{aligned}$$

These equations can be rearranged to show more explicitly the dependence on ωt_o. Dropping the subscript 1,

$$y_{sc}=\left(\frac{eV_{AC_o}}{md\omega^2}\right)\Bigg\{\left[2+\delta^2+2\delta^2k+2k^2\delta^2-2(1+k\delta^2+k^2\delta^2)\cos\delta-2\delta\sin\delta\right]^{\frac{1}{2}}\cdot\sin\Big(\omega t_o$$

$$+\tan^{-1}\left[(\delta(1+k)-k\delta\cos\delta-\sin\delta)/(1-\cos\delta+k\delta\sin\delta)\right]\Big)$$

$$+\left(\frac{\delta}{2}\right)^2\left[\left(\frac{V_{DC_1}}{V_{AC_o}}\right)\left(\frac{1}{2}+2k\right)+\left(\frac{V_{DC_2}}{V_{AC_o}}\right)\left(\frac{1}{2}+2k\right)\right]\Bigg\}$$

$$\equiv\left(\frac{eV_{AC_o}}{md\omega^2}\right)\Big\{A(\delta,k,V_{AC_o},V_{DC_1},V_{DC_2})+B(\delta,k)\sin[\omega t_o+\theta(\delta,k)]\Big\} \qquad (12)$$

where

$$A=\left(\frac{\delta_1}{2}\right)^2\left[\left(\frac{V_{DC_1}}{V_{AC_o}}\right)\left(\frac{1}{2}+2k\right)+\left(\frac{V_{DC_2}}{V_{AC_o}}\right)\left(\frac{1}{2}+2k\right)\right]$$

$$B=\left[2+\delta^2+2\delta^2k+2k^2\delta^2-2(1+k\delta^2+k^2\delta^2)\cos\delta-2\delta\sin\delta\right]^{\frac{1}{2}}$$

$$\theta=\tan^{-1}\left[\left(\delta(1+k)-k\delta\cos\delta-\sin\delta\right)/(1-\cos\delta+k\delta\sin\delta)\right]$$

$$k=l_2/l_1$$

Thus

$$\frac{dy_{sc}}{dt_o}=\left(\frac{eV_{AC_o}}{md\omega}\right)\left[B(k\delta)\cos(\omega t_o+\theta(k\delta))\right] \qquad (13)$$

FIGURE 7. ION DISPLACEMENT AS FUNCTION OF ENTRANCE PHASE ANGLE AND TRANSIT PHASE ANGLE FOR SIMPLE DEFLECTOR PLATES

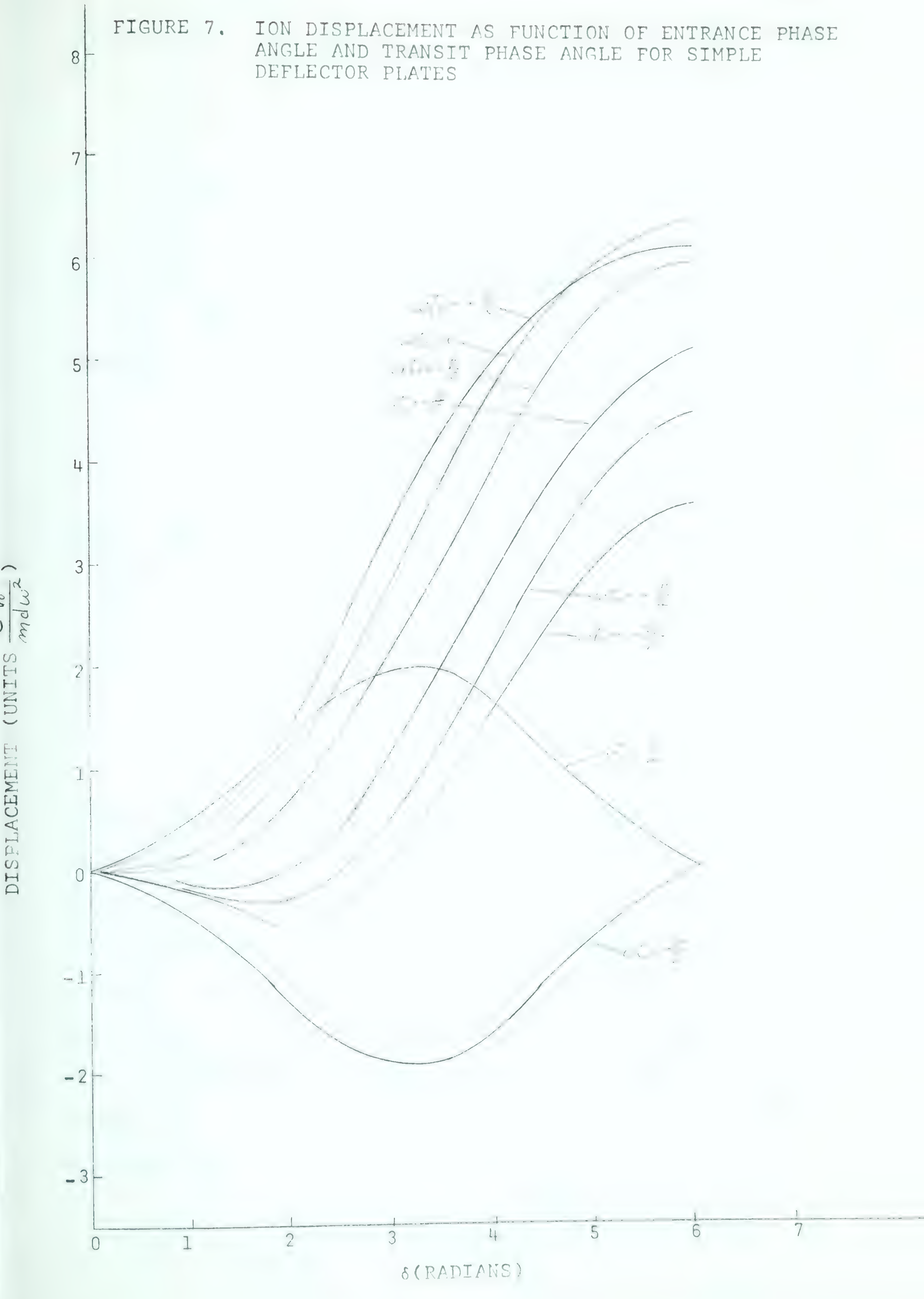

Figure 7 shows the trajectory between plates for which the d.c. biases are zero, or alternately the displacement of an axial ray produced at the exit of plates of effective length "δ". Figure 8 shows the corresponding $y(\delta_1, \omega t_0)$.

The total dependence of Equation 12 on the d.c. bias is contained in the coefficient A. For zero d.c. bias A = 0.

(i) Zero d.c. Bias on Deflection Plates

Consider the case of zero bias. Therefore, $A(\delta, k, \ldots) = 0$, and we have for $y_{sc} = 0$ $\sin(\omega t_0 + \theta) = 0$ or $\cos(\omega t_0 + \theta) = 1$. It follows that

$$\Delta t_0 = \Delta y_{sc} \Big/ \left[(eV_{AC_0}/wmd)\, B(\delta k) \right] \qquad (14)$$

$$= \Delta y_{sc} / w.s.$$

As $\cos(\omega t_0 + \theta) = 0$, the entrance phase angle ωt_0 is determined by θ. Equation (12) shows that the writing speed varies in a sinusoidal manner with the angular velocity of the impressed a.c. voltage. The dependence of the writing speed on the parameters δ (plate length), and k(lever arm) is contained in the coefficient $B(\delta, k)$. Figure 9 gives this dependence. The writing speed is seen to be a maximum for δ slightly greater than 4. For small δ, from Equation 14

$$\frac{\Delta y_{sc}}{\Delta t_0} = \left(\frac{eV_{AC_0}}{wmd}\right) B(\delta k) \approx \frac{1}{4} \left(\frac{\omega e V_{AC_0}}{Ed}\right) l_1 (l_1 + 2 l_2)$$

FIGURE 8. TRANSVERSE VELOCITY VS. PLATE LENGTH

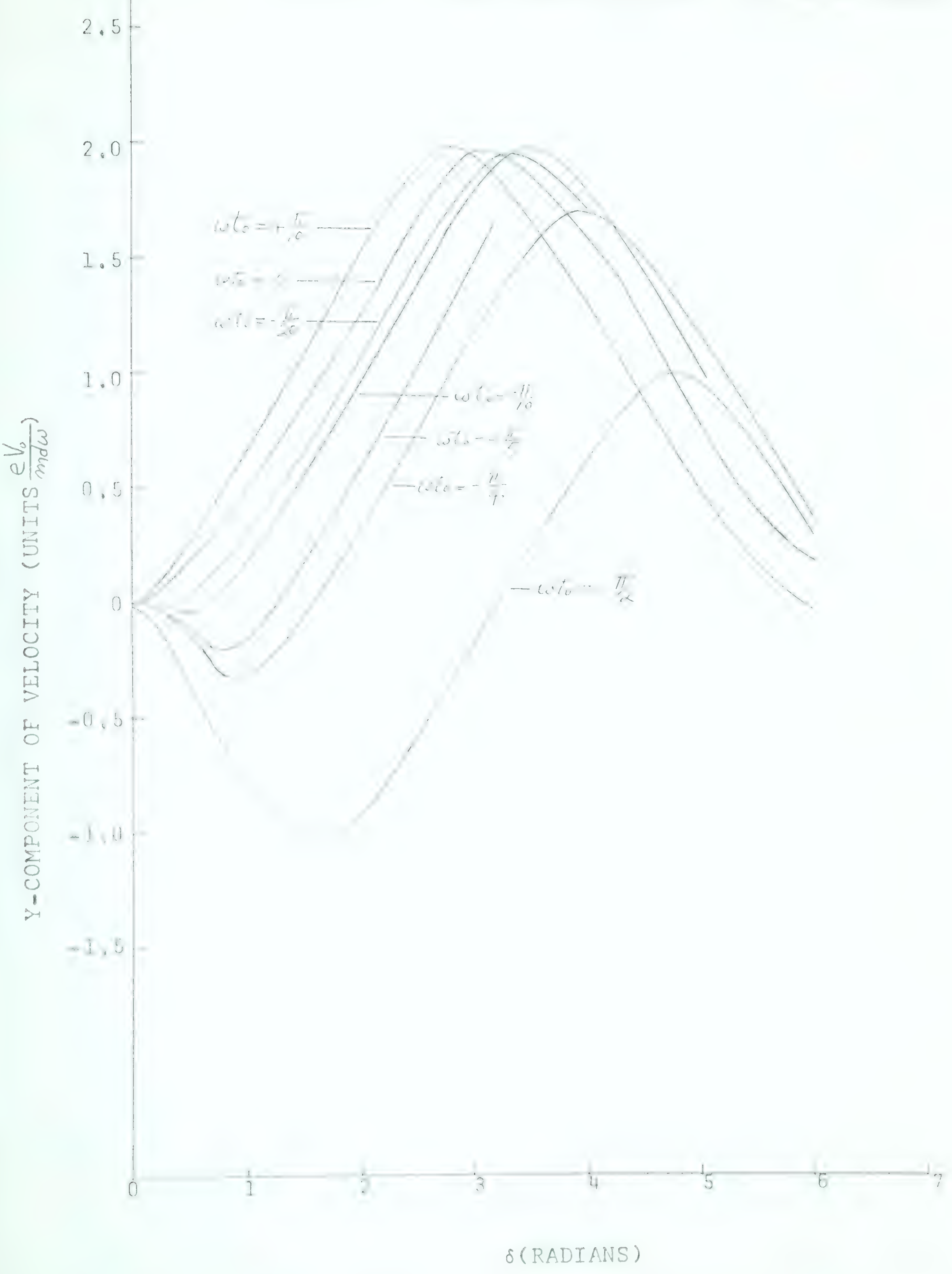

FIGURE 9: W.S. vs PLATE LENGTH

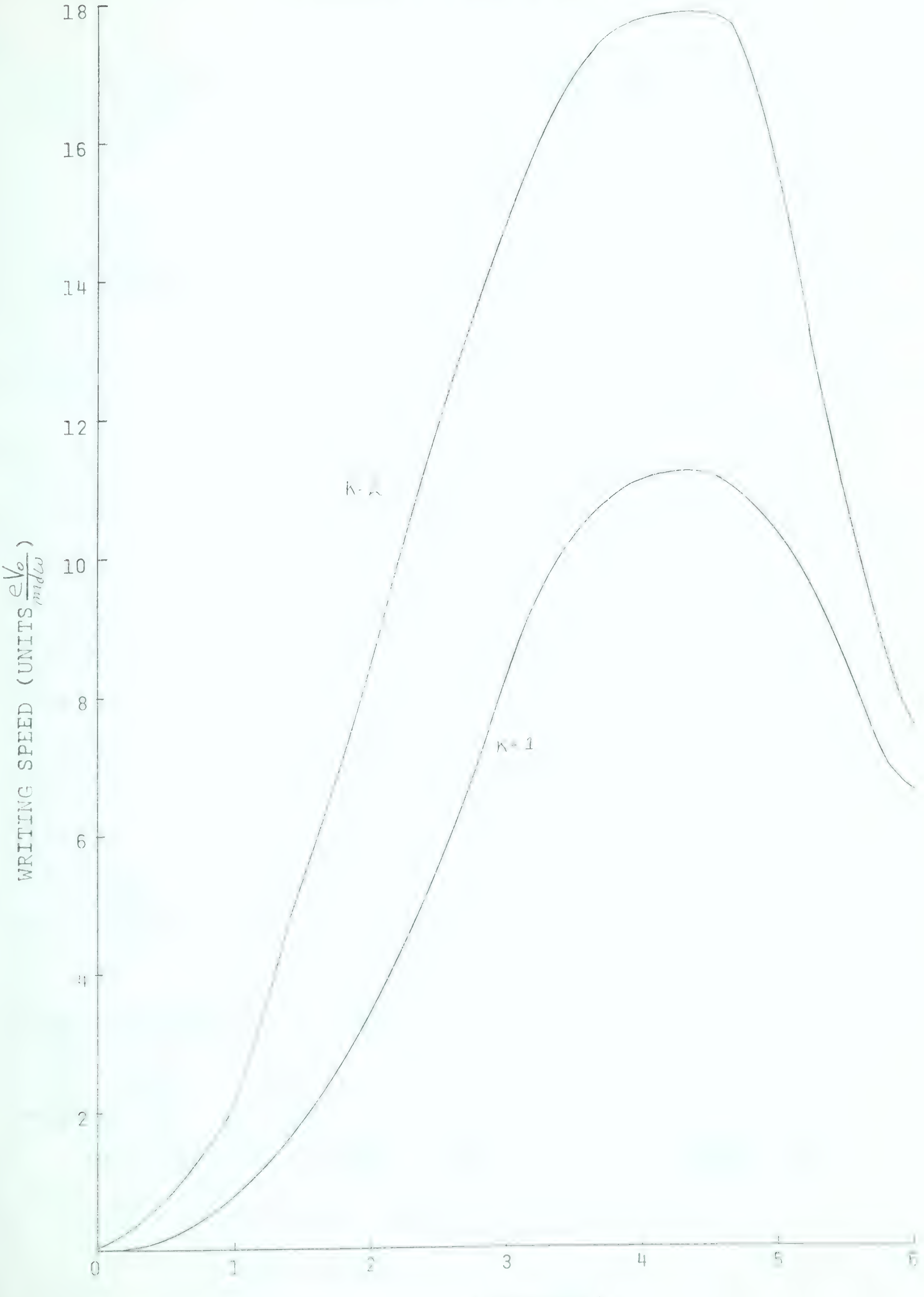

which gives us the value obtained from the simple theory (Equation 6).

(ii) Non Zero D.C. Bias on Deflection Plates

Returning to the case of d.c. bias on the plates we see from Equations 12 and 13 that the writing speed is reduced for $A \neq 0$, since $\cos(\omega t_o + \theta) < 1$, though this is not the purpose of these voltages.

We see from Equation 12 that when ωt_o has advanced by π y_{sc} is again zero. But Equation 11 says that both y and $\dot{y}$ change sign when ωt_o is increased by π. Thus there are two beams from the simple deflector plate system. They show a symmetry which exists when the beam defining slit (Figure 6) is on axis. Now if the aperture is effectively moved off axis by the use of d.c. biases, $A \neq 0$, the condition $y_{sc} = 0$ can be met, using arbitrary values of $y(\delta,\ldots)$, by suitable d.c. biasing. Let the argument of $\sin(\omega t_o + \theta)$ be α for $y_{sc} = 0$. Then an increase in α to $(\pi-\alpha)$ again leads to $y_{sc} = 0$, and the above symmetry has been removed as we now have two different values for y and also for $\dot{y}$. This principle may be employed in permitting the acceptance of only one of the two ion bursts produced per r.f. cycle. A system of refractor plates separate from the sweeping plates will be considered later.

It is possible by proper choice of the d.c. biases to

have $y(\delta,\ldots) = \dot{y}(\delta,\ldots) = 0$ so that the beam enters as an axial beam and leaves the pulsing system as a mean axial pulse. The alternate pulse will be off axis sufficiently to remove with defining slits, leaving the axial path unaltered.

The two conditions $y_{sc} = 0$ with zero bias, and $y_{sc} = 0$ with biases set to make $y(\delta,\ldots) = \dot{y}(\delta,\ldots) = 0$ establish the following relations between ωt_0 and δ.

$$\omega t_0 = -\tan^{-1}\left[(\delta(1+k) - k\delta\cos\delta - \sin\delta)/(1-\cos\delta + k\delta\sin\delta)\right] \tag{15a}$$

$$\frac{V_{DC_1}}{V_{AC_0}} = \left[2(1-\cos\delta)/\delta\right]^{1/2}\sin\left(\omega t_0 + \tan^{-1}\left[(1-\cos\delta)/\sin\delta\right]\right) - (4/\delta^2)\left[(1-\cos\delta)^2 + (\delta-\sin\delta)^2\right]^{1/2}\cdot\sin\left(\omega t_0 + \tan^{-1}\left[(\delta-\sin\delta)/(1-\cos\delta)\right]\right) \tag{15b}$$

with

$$\frac{V_{DC_2}}{V_{AC_0}} = -\left[\frac{V_{DC_1}}{V_{AC_0}} + \left(\frac{2}{\delta}\right)\left[2(1-\cos\delta)\right]^{\frac{1}{2}}\sin\left(\omega t_0 + \tan^{-1}\left[(1-\cos\delta)/\sin\delta\right]\right)\right]$$

Figures 10 and 11 show the relationships 15a and 15b respectively.

(b) Energy Spread of an Axial Monoenergetic Beam Due to a Finite Entrance Time

This section pertains to the effects on the beam element which enters the sweeping system during the acceptance time

FIGURE 10. ωt_o vs. PLATE LENGTH WITH K AS PARAMETER

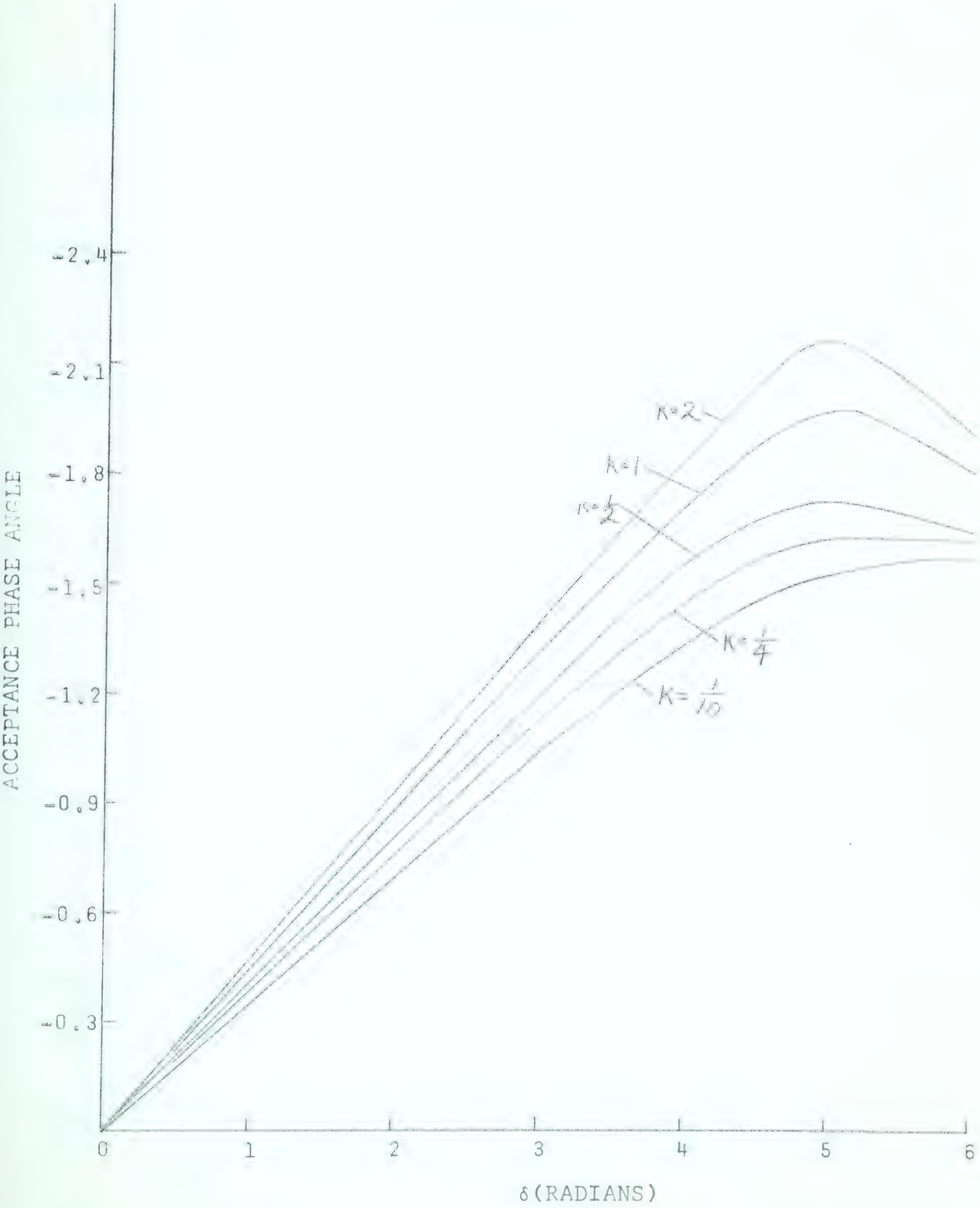

FIGURE 11. ωt_o vs PLATE LENGTH WITH $\frac{V_{DC_1}}{V_{AC_o}}$ AS PARAMETER

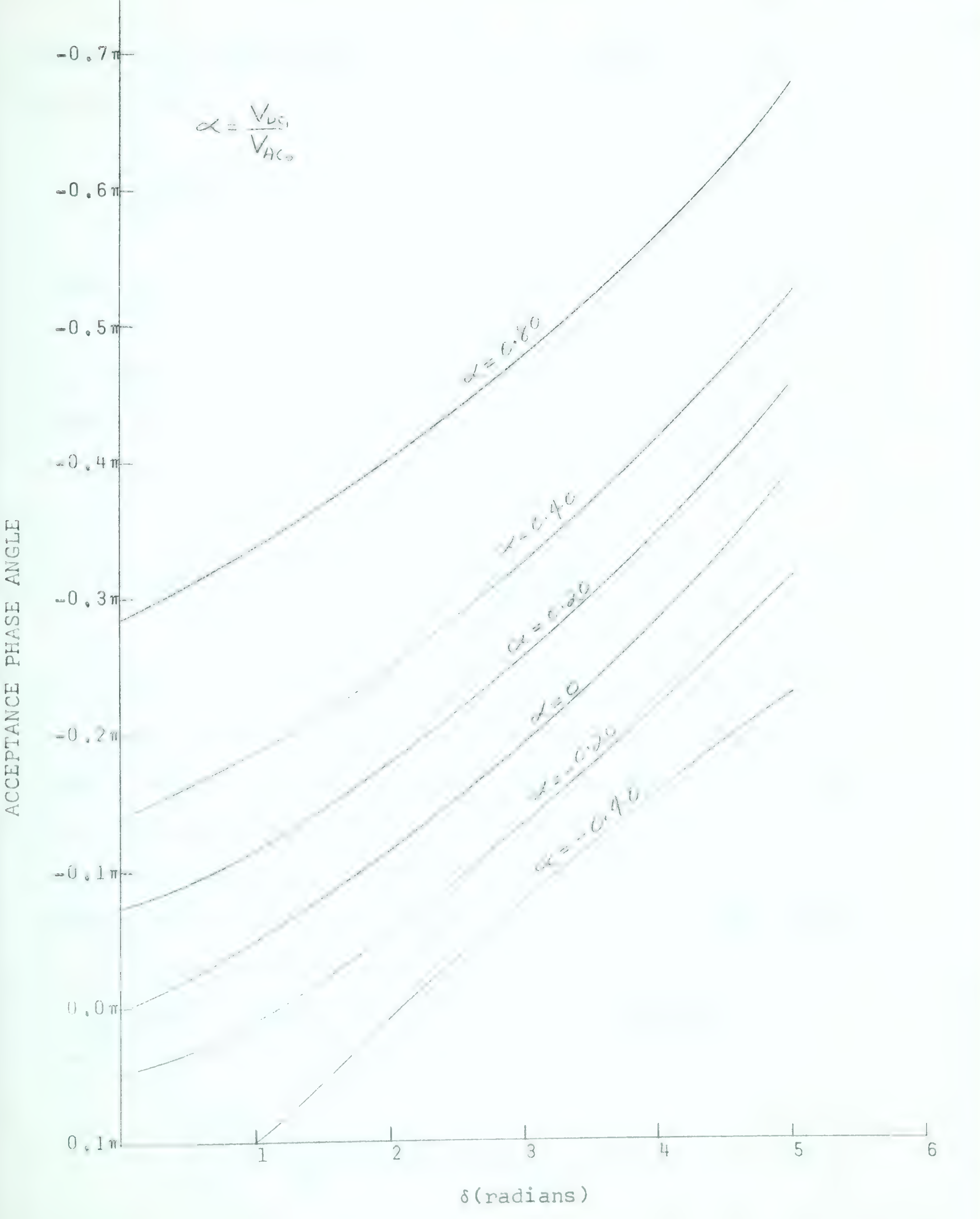

period dt_0. This discussion will be limited to the case of zero bias. We may rewrite Equation 2 as

$$y(\ell_1) + \tau_2\,\dot{y}(\ell_1) = 0 \qquad (2b)$$

where τ_2 is considered a constant. Now from Equation 9 we see that both $y(\ell_1)$ and $\dot{y}(\ell_1)$ change with t_0, so one of the changes occurring during the time period dt_0 is a change in the direction of the beam. If H = KE + PE is the total energy of the pulse at the exit of the plates (ℓ_1) we have

$$dH = d(P.E.) = \frac{\partial V(\ell_1)}{\partial t}\,dt = \left(\frac{y(\ell_1)}{d}\right)\frac{dV}{dt}\,dt$$

where $V(\ell_1)$ is the instantaneous voltage across the sweeping plates and $y(\ell_1)$ the distance of the pulse off axis at time $t = t_0 + \tau_1$. Thus particles which emerge $dt = dt_0$ apart have respectively increasing or decreasing energies as the potential is rising or falling with time. It has been shown that as the particle exits from the plates it is experiencing an increasing positive potential, thus the particle arriving at the exit dt_0 behind another receives an increase in energy over the first particle given by

$$\frac{y(\ell_1)}{d}\,\frac{dV(t)}{dt}\,dt_0$$

This difference in total energy becomes a difference in kinetic energy in the field free region from the plates to the beam defining slits. This results in a time-energy correlation of the pulse with the more energetic particles occurring last; thus there is a possibility of bunching occurring at the target.

The arrival time of the particles at the screen t_{sc} is given by

$$t_{sc} = t_0 + \tau_1 + \tau_2 . \qquad (16)$$

Formerly with Equation 2b we had $dt_{sc} = dt_o$, the entrance time spread of the initial beam burst, for two particles of the same energy entering the plates dt_o apart. Now $\Delta\tau_1 = 0$ because the KE of both particles is the same after they enter the plates, on axis. Also $\Delta\tau_2 = 0$ by the assumption of Equation 2b. But we have shown that an energy spread exists in the pulse upon its exit from the plates. This energy spread will lead to varying times of arrival of the pulse particles.

$$\Delta\tau_2 = -\frac{1}{2}\,\frac{\Delta E(l_1)}{E}\,\tau_2 = -\frac{1}{2}\,\frac{e\,y(l_1)}{d}\,\frac{\delta V(t_0+\tau_1)}{\delta t}\,\Delta t_0\,\frac{\tau_2}{E} \qquad (17)$$

Thus from Equation 16

$$\Delta t_{sc} = \Delta t_0 - \frac{\Delta t_0}{2}\left(\frac{e\,y(l_1)}{d}\right)\left(\frac{\delta V}{\delta t}\right)\left(\frac{\tau_2}{E}\right) . \qquad (17a)$$

Hence, although τ_2 is considered to be constant in estimating the writing speed, its small variance makes bunching of the pulse occur under the condition in Equation 17a that $\Delta t_{sc} = 0$. The condition on $\Delta\tau_2$ can be stated as

$$\dot{y}(l_1)\,\Delta\tau_2 \ll y(l_1) + \tau_2\,\dot{y}(l_1) \tag{18}$$

$$\equiv \text{writing speed} \cdot \Delta t_o .$$

Both equation (17a) and (18) can be reasonably well satisfied simultaneously.

C. Finite Sized Parallel Exit Beam

Equation 11 may be rewritten (Tu 58) for the case of zero biases as

$$y_{sc} = \left(\frac{eE_o}{m\omega^2}\right)\Big\{\cos\delta_o\left[\delta_1 - \sin\delta_1 + \delta_2(1-\cos\delta_1)\right] + \sin\delta_o\left[1-\cos\delta_1 + \delta_2\sin\delta_1\right]\Big\}. \tag{11a}$$

If we let δ_o be $\left(-\frac{\delta_1}{2}+\theta\right)$ with $\theta << 1$ (19)

$$y_{sc} = \frac{eE_o}{m\omega^2}\Big\{\left[-2\sin\frac{\delta_1}{2} + \delta_1\cos\frac{\delta_1}{2}\right] + \left[\theta(1+2k)\,\delta_1\sin\frac{\delta_1}{2}\right]\Big\}. \tag{20}$$

The formula for the burst length may be obtained by substituting in the limiting values set by the slit aperture and the

beam burst diameter at the slits. The burst duration is given by the difference in the two corresponding values of θ. Let d be the slit width and W the beam diameter. Thus the two extreme conditions of Equation 12 give:

$$\left(\frac{d}{2}+\frac{W}{2}\right)=\left(\frac{eE_0}{m\omega^2}\right)\left\{\left[-2\sin\frac{\delta_1}{2}+\delta_1\cos\frac{\delta_1}{2}\right]+\left[\theta_1(1+2k)\,\delta_1\sin\frac{\delta_1}{2}\right]\right\},$$

$$\left(-\frac{d}{2}-\frac{W}{2}\right)=\left(\frac{eE_0}{m\omega^2}\right)\left\{\left[-2\sin\frac{\delta_1}{2}+\delta_1\cos\frac{\delta_1}{2}\right]+\left[\theta_2(1+2k)\,\delta_1\sin\frac{\delta_1}{2}\right]\right\}, \tag{21}$$

$$(\theta_1-\theta_2)=\frac{(d+W)\,m\omega^2}{eE_0\,\delta_1}\,\frac{1}{(1+2k)\sin\delta_1/2},$$

i.e.

$$\Delta t_{sc}=\frac{m(d+W)\,(1+k)}{eE_0\tau_0\,(1+2k)\sin\frac{\delta_1}{2}},$$

where

$$\tau_0=\tau_1+\tau_2=\tau_1(1+k).$$

Alternatively by differentiating with respect to θ

$$\frac{dy_{sc}}{d\theta}=\frac{eE_0}{m\omega^2}\,(1+2k)\,\delta_1\sin\frac{\delta_1}{2}\qquad;\ d\theta=\omega\Delta t_{sc}.$$

Therefore, again

$$\Delta t_{sc}=\frac{m(d+W)}{eE_0\tau_0}\,\frac{1+k}{(1+2k)\sin\frac{\delta_1}{2}}=K\,\frac{(1+k)}{(1+2k)\sin\frac{\delta_1}{2}},$$

where we take the slit width plus the beam width to be the effective beam defining aperature and $K = m(d + W)/(eE.t_o)$. In deriving (21) it was assumed that δ_1 and δ_2 are constants.

It is seen that for K constant, the burst length can never be less than K/2. Also for any given frequency there is an optimum value of k given by finding the minimum of $\Delta T_{sc}/K$. As a function of k

$$\Delta t_{sc}/K = \frac{1+k}{(1+2k)\sin\left[\frac{\delta'}{2(1+k)}\right]}$$

and $\delta' = \delta_1 + \delta_2 = \delta_1(1+k)$.

k_{opt} is given by

$$\tan\delta'' = \delta''(1+2k_{opt}), \qquad (22)$$

where $\delta'' = \delta'/[2(1+k_{opt})]$.

Figure 12 shows a plot of k_{opt} vs δ_0.

(d) Non Parallel Exit Beam of Finite Size

(i) Simple Geometrical Consequence of Beam Divergence on the Writing Speed

The divergent exit beam of a parallel incident beam may be described by the equation

$$r = r_0 + \alpha l_2$$

FIGURE 12. K_{opt} vs δ_0

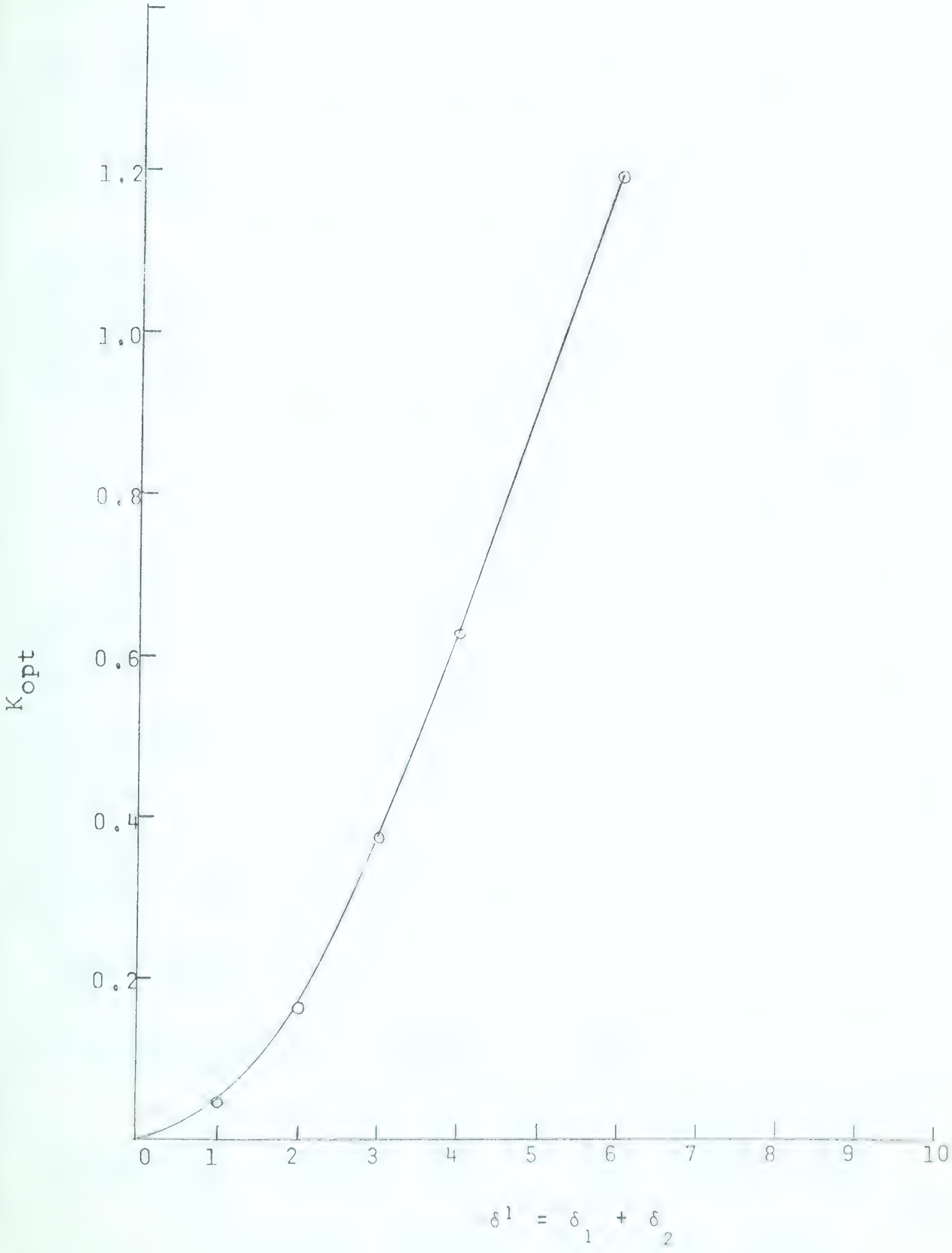

where r is the beam radius, l_2 is the distance from the plates to the slits, and α is the small half angle divergence of the beam. Now if $l_2 \alpha >> \dot{r}_0$, and since $l_2 = k l_1$ one has from Equation 21, with $W \equiv r$,

$$dt_0 \approx \text{constant} \;\; x \; k l_1 \alpha / B(k\delta).$$

Thus dt_0 increases with k. This simple argument shows that the writing speed cannot be indefinitely increased by increasing k.

(ii) Negligible Voltage Gradient Across the Ion Beam

Effects of beam cross-section and divergence will be considered under the assumption that the plates are short, the voltage across the plates low, or the beam cross-section small, but finite. Consider a parallel beam of radius Δy_0, with outside rays converging to radius a at the screen. The slits will be considered a point aperture on axis. For an axial ray

$$y_{sc} = y(l_1) + \tau_2 \dot{y}(l_1) = \frac{eV_0 B(\delta k)}{md\omega^2} \sin(\omega t_0 + \theta).$$

For a ray entering the sweeping plates with $y = \Delta y_0$, $y = y_0$,

$$\begin{aligned} y_{sc}(\Delta y_0, \dot{y}_0) &= y(l_1) + \dot{y}(l_1)\tau_1 + \Delta y_0 + \tau_2[\dot{y}(l_1) + \dot{y}_0] \\ &= y(l_1) + \tau_2 \dot{y}(l_1) + \dot{y}_0(\tau_1 + \tau_2) + \Delta y_0 \end{aligned} \qquad (19)$$

$$= y_{sc\,(axial)} + \dot{y}_0(\tau_1 + \tau_2) + \Delta y_0 .$$

Assuming that $y_{sc}(y_0, \dot{y}_0)$ can be represented by the first two terms in the Taylor expansion about the angle $(\omega t_0 + \theta) \approx 0$, as the aperture is on axis.

$$y_{sc}(\Delta y_0, \dot{y}_0) = \left(\frac{eE_0B}{m\omega^2}\right) \sin\left[\omega(t + \Delta t_0) + \theta\right] \tag{20}$$

$$\approx \left(\frac{eE_0B}{m\omega^2}\right) \sin(\omega t_0 + \theta) + \Delta t_0 \frac{eE_0B}{m\omega^2} \omega \cos(\omega t_0 + \theta). \tag{21}$$

Comparing Equations 19 and 21

$$\frac{eE_0B}{m\omega^2} = \cos(\omega t_0 + \theta)\, \omega\, \Delta t_0 = \dot{y}(\tau_1 + \tau_2) + \Delta y_0 . \tag{22}$$

Now as $\cos(\omega t_0 + \theta) \approx 1$

$$\Delta t_0 = \left(\dot{y}(\tau_1 + \tau_2) + \Delta y_0\right) / w.s. \tag{22a}$$

where w.s. is the writing speed (Equation 14).

From Equation 19 and the initial conditions

$$a = \dot{y}_0(\tau_1 + \tau_2) + \Delta y_0 .$$

Thus

$$\Delta t_o \approx \frac{a}{w.s.} \cdot \tag{23}$$

If Δt_{o+-} is the total time for the entire beam to cross the infinite aperture

$$\Delta t_{o+-} = 2a/w.s.$$

If the beam emerges from the plates as a parallel beam

$$\Delta t_{o+-} = 2\,\Delta y_o/w.s. \tag{24}$$

This justifies taking $y_{eff} = d + W$.

(iii) Significant Voltage Gradient Across the Ion Beam

Now the conditions of short plates, low voltage, or small beam cross-section will be lifted. These conditions maintain a small voltage difference across the entering beam.

Consider an incident, parallel, monoenergetic beam of radius Δy_o. Let τ_1 be the transit time of an axial ray. Then

$$\tau_{1+} = \tau_1 + d\tau_1 \text{ and } \tau_{1-} = \tau_1 - d\tau_1 .$$

will be the transit times of the extreme rays entering respectively at higher and lower potentials than the axial rays. It is seen that $\tau_{1+} > \tau_1' > \tau_{1-}$. Incident axial rays with the transit times above would, in the field free region beyond the plates, have the kinetic energy

$$T_1 - \left[dE_1 - \frac{\delta V(y,t)}{\delta t}\, d\tau_1\right] , \quad T_1 \quad , \quad T_1 + \left[dE_1 - \frac{\delta V(y,t)}{\delta t}\, d\tau_1\right]$$

respectively, and they would emerge in the sequence τ_-, τ, τ_+.

For the ray τ_{1-} entering the deflection plates according to Equations (22), (23), and (24) the plate exit time is $(\Delta y_o/ws - \Delta\tau_1/2)$ with respect to τ_1 (Ne 60). One finds the difference in total energy at l_1 corresponding to the diameter of the beam as

$$\Delta H(l_1)_+ \simeq 2e\left\{ \frac{y(l_1)}{d}\frac{\delta V(t)}{\delta t}\left(\Delta y_o/w.s. - \frac{\Delta\tau_1}{2}\right) \right. \qquad (25)$$

$$\left. + \frac{\Delta y_o}{d}\left|V(t_o)\right| + \frac{\Delta y_o}{d} V(t)\right\}$$

where $\Delta\tau_1 \simeq \frac{1}{4}\left(\frac{weV_o}{E}\right)\tau_1^2\, \frac{\Delta y_o}{d}$.

Therefore

$$\Delta t_{sc+-} = \Delta t(l_1) - \frac{1}{2}\left(\frac{\Delta H(l_1)}{E}\right)\tau_2$$

$$= \left[2 - e\left(\frac{\tau_2}{E}\right)\left(\frac{y(l_1)}{d}\right)\left(\frac{\delta V}{\delta t}\right)\right]\left(\Delta y_o/w.s. - \frac{\Delta\tau_1}{2}\right) \qquad (26)$$

$$- e\left[\left|V(t_o)\right| + V(t)\right]\left(\frac{\Delta y_o}{d}\right)\left(\frac{\tau_2}{E}\right).$$

If the term $(e\tau_2/E)\,(y(l_1)/d)\,(\delta V/\delta t)$ may be neglected, as when the deflector plates are short

$$\Delta t_{sc} \simeq 2\Delta y_0/_{W.S.} - \frac{2eV(t)\,\Delta y_0\,\tau_2}{Ed} - \Delta\tau_1 \,. \qquad (26a)$$

(a) Time Focussing

Time focussing on a small aperture gives

$$\frac{1}{W.S.} - \frac{e\,V(t)\,\tau_2}{Ed} - \frac{1}{8}\,\frac{\omega e V_0}{Ed} = 0 \,. \qquad (27)$$

Thus the finite aperture yields the same burst duration as an axial ray, but induces an energy spread given by Equation (25).

(b) Space Focussing

Alternately space focussing gives

$$\Delta t_{sc\,+-} \simeq 0 - 2\Delta y_0 \left(\frac{eV_0}{Ed}\right)\left(\tau_2 + \frac{1}{8}\omega\tau_1^{\,2}\right).$$

Here Δt_{sc}+- may be made small by diminishing τ_1 and τ_2.

(e) Initial Energy Spread in Ion Beam

Now an initial energy spread ΔE will be introduced into an axial ray, and its effects at a point aperture considered.

Now

$$t_{sc} = t_0 + \tau_1 + \tau_2$$

and

$$dt_{sc} = dt_0 + d\tau_1 + d\tau_2 .$$

From Figure 6 we see that $dt_0 \approx -\frac{1}{2}\ d\tau_1$ where $|d\tau_1| = \frac{1}{2}\frac{\Delta E}{E}\tau_1 .$

Therefore Δt_{sc}(energy spread) =

$$\left(\frac{1}{2}+k\right) d\tau_1 = \frac{1}{2}\left(\frac{1}{2}+k\right)\frac{\Delta E}{E}\tau_1 . \qquad (28)$$

Thus the initial energy spread restricts the burst time duration at the slits.

(f) Theory of Refractor Plate Action

The operation of refractor plates (Tu 58) is based on the radial displacement of the beam during the upsweep and downsweep. It is possible to form a dimensionless ratio between the two formulae

$$y_{sc} = \left(\frac{eE_{AC_0}}{m\omega^2}\right)\left\{\left[-2\sin\frac{\delta_1}{2} + \delta_1\cos\frac{\delta_1}{2}\right] + \left[\theta(1+2k)\delta_1\sin\frac{\delta_1}{2}\right]\right\} \qquad (29)$$

and $$\dot{y}_{sc} = \frac{2eE_{HC_0}}{m\omega}\theta\sin\frac{\delta_1}{2} . \qquad (30)$$

Viz: $$\frac{(y_{sc} - b)}{a} = \frac{\dot{y}_{sc}}{v_0} . \qquad (31)$$

Comparing 31 with 29 and 30

$$b = \left(\frac{eE_{AC_0}}{m\omega^2}\right)\left[-2\sin\frac{\delta_1}{2} + \delta_1 \cos\frac{\delta_1}{2}\right] \tag{32}$$

and $$a = \frac{1}{2} v_0 \left[\tau_1 + 2\tau_2\right] \equiv \frac{v_0}{2\omega}\delta_1 (1+2k). \tag{33}$$

This value of a indicates that the virtual source (Figure 13) is located half way along the plates. It is also seen from Figure 13 that the virtual source is located the distance b below axis during an upsweep and above axis for the downsweep.

The action of the refractor plates is shown in Figures 13a and 13b. The d.c. biases displace the virtual source vertically.

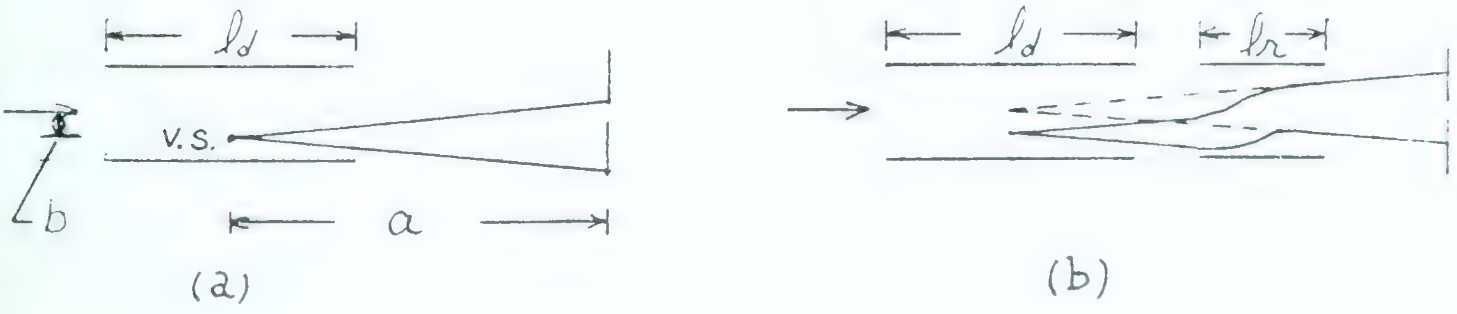

Figure 13. Schematic Representation of Traces of Upswept Beam Traversing Deflecting Plates; (a) without Refractor Plates, (b) with Refractor Plates.

(a) Within the deflector plates

$$y = \left(\frac{eE_0}{m\omega^2}\right)\left\{\sin\omega t_0 - \sin\omega t + \omega\tau_1\cos\omega t_0\right\}$$

$$\dot{y} = \left(\frac{eE_0}{m\omega}\right)\left\{\cos\omega t_0 - \cos\omega t\right\}.$$

Beyond the deflector plates $\left(\tau_2 > \frac{l_{r3}}{v_0} = \tau_r + \tau_3\right)$

$$y_n = y(l_1) + \tau_2\,\dot{y}(l_1)$$

$$= \left(\frac{eE_0}{m\omega^2}\right)\left\{\sin\omega t_0 - \sin\omega t_1 + \omega\tau_1\cos\omega t_0\right\}$$

$$+ \left(\frac{eE_0}{m\omega}\right)(\tau_r + \tau_3)\left\{\cos\omega t_0 - \cos\omega t_1\right\}.$$

(b) Within refractor plates

$$y = \frac{eE_r}{m}\left(\frac{\tau_2}{2}\right)^2 + \frac{eE_0}{m\omega}\left\{\cos\omega t_0 - \cos\omega t_1\right\}(\tau_2)$$

$$+ \frac{eE_0}{m\omega^2}\left\{\sin\omega t_0 - \sin\omega t_1 + \omega\tau_1\cos\omega t_0\right\}$$

$$\dot{y} = \frac{eE_r}{m}\tau_2 + \frac{eE_0}{m\omega}\left\{\cos\omega t_0 - \cos\omega t_1\right\}.$$

Beyond refractor plates

$$y_r = \frac{1}{2}\left(\frac{eE_r}{m}\right)\tau_2^2 + \left(\frac{eE_0}{m\omega}\right)\tau_2(\cos\omega t_0 - \cos\omega t_1)$$

$$+ \left(\frac{eE_0}{m\omega^2}\right)\left\{\sin\omega t_0 - \sin\omega t_1 + \omega\tau_1\cos\omega t_0\right\}$$

$$+ \tau_3\left\{\frac{eE_r}{m}\tau_2 + \frac{eE_0}{m\omega}(\cos\omega t_0 - \cos\omega t_1)\right\}$$

where τ_3 is the time lapsed since the particle left the refractor plates.

Subtracting y_r from y_n

$$y_n - y_r = \frac{1}{2}\frac{eE_r}{m}\tau_2^2 + \tau_3\left(\frac{eE_r}{m}\tau_2\right).$$

To obtain the virtual displacement of b we must extend τ_3 back in time to $\tau_1/_2$ obtaining:

$$|b| = \frac{1}{2}\,\frac{eE_r}{m}\,\tau_r(\tau_r+\tau_1) \equiv \frac{eE_r}{2m\omega^2}\,\delta_r(\delta_r+\delta_1)$$

where E_r is the d.c. bias on the refractor plates. If two sets of refractor plates are used, having the same lengths but oppositely directed d.c. fields, one finds that

$$|b| = \frac{eE_r}{m\omega^2}\,\frac{(\delta_r)^2}{4}.$$

Although the double set of plates works better, the single plate has the advantage of simplicity and of requiring less voltage for a given overall length.

As the action of the refractor plates is in the same direction for both upsweeps and downsweeps, the adjustment of one virtual source on axis automatically displaces the other virtual source further off axis. Thus the transmission of one beam burst makes it easier to eliminate the alternate beam burst with slits.

The previous discussion has described various properties

of a deflector plate, beam chopping system. A brief summary of these properties follows.

For an axial, monoenergetic ray swept between the deflector plates by a sinusoidally varying voltage; (a) the "chopping" introduces into the ray a time-correlated variation in angle and energy as the ray scans the aperture; (b) the last particles to leave the deflector plates have the higher energy; (c) there is an optimum value for the plate length which leads to a maximum writing speed; (d) the ion burst duration is explicitly a function of the transit time (δ_1) of the system. Thus "chopping systems" for various energy beams are similar if the transit times are similar. The effect of a finite diameter of a parallel beam is that (e) the beam dimension introduces a time spread at each point of a finite aperture; (f) the time duration at each point of the finite aperture has a correlated energy variation, in that the latter particles leaving the deflector plates have higher energy. Thus the beam can be time focussed, giving a burst length equal to that of an axial ray. The effect of an initial energy spread is that (g) a time spread occurs at the screen which limits the shortness of burst obtainable.

(C) Klystron Bunching

1. Simple Theory

Here the basic principle is to speed up the last ions

of the group so that they catch up with the first ions at a given point. A sinusoical voltage

$$V = V_b \sin \omega t$$

is applied across an acceleration gap, G.

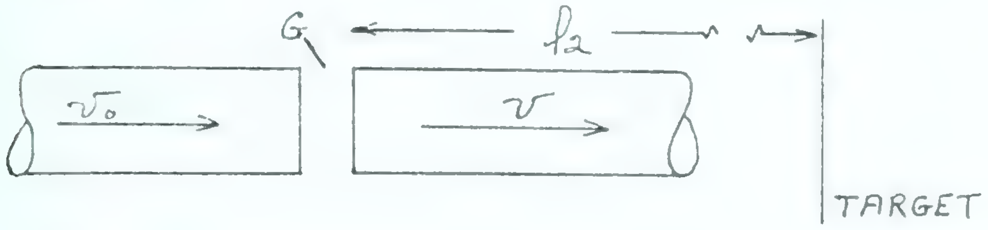

The ion energy is given by

$$\tfrac{1}{2} m v^2 = e(V_0 + V_b \sin \omega t_1) \quad ; \quad eV_0 = \tfrac{1}{2} m v_0^2$$

so

$$v = v_0 (1 + \alpha \sin \omega t_1)^{\frac{1}{2}} \quad ; \quad \alpha = V_b / V_0$$

$$\approx v_0 (1 + \tfrac{\alpha}{2} \sin \omega t_1) \quad ; \quad \alpha << 1$$

t_1 = time beam passes G

t_2 = time beam hits target.

Now

$$t_2 = t_1 + \frac{l_2}{v_0}(1 - \tfrac{\alpha}{2} \sin \omega t_1)$$

so

$$dt_2 = dt_1 (1 - M \cos \omega t_1) \quad ; \quad M = (\omega \alpha l_2)/(2 v_0).$$

For

$$\cos \omega t_1 \approx 1 \, , \quad M = 1 \, .$$

$$dt_2 = 0 \, .$$

The major difficulties with this system are that bunching occurs only over a short period of the cycle, thus the initial pulse length must be fairly short. Also an energy spread given approximately by

$$\Delta E_1 \cdot \Delta t_1 = \Delta E_2 \cdot \Delta t_2$$

is introduced into the beam.

2. Extended Theory

The intention here is to bunch an ion beam produced by an r.f. ion source. Pre-acceleration bunching will be attempted as it permits use of smaller modulating voltage amplitudes. The system to be used consists of an r.f. ion source, a buncher tube, an accelerator tube, and finally a drift tube. Ideally all the bunching should occur within the bunching tube and the bunched beam then accelerated to its target as quickly as possible to reduce space charge effects. In practice, however, some bunching will occur in both the accelerator and drift tubes. The form of the modulating voltage is given below.

First consider bunching across a single gap, G. Let the initial field on the buncher be E_o for $t < 0$. The flight time through the buncher tube is $T_o = \left(\sqrt{m/2}\;\ell\right)/\sqrt{E_o}$

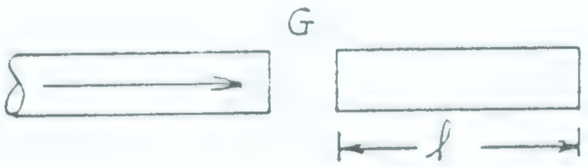

Figure 14. Simple Bunching System

Now for $t \geqslant 0$ a modulating voltage is applied and the field in the buncher tube becomes $E_0 + \Delta E(\tau)$. Let t_1 be the time the last particle of the pulse crosses the acceleration gap. For bunching we would like the particle crossing the acceleration gap at $t_0 = 0$ to arrive at the exit of the buncher tube at the same time as the particle crossing this gap at $t = t_1$. For the first particle we have $\sqrt{E_0} = \sqrt{m/2}\, \ell_1/T_0$ as the time to travel the distance ℓ_1. The last particle must traverse ℓ_1 in the time $T_0 - t_1$ for perfect bunching; hence $\sqrt{E_0 + \Delta E} = \sqrt{m/2}\, \ell_1/(T_0 - t_1)$ will give the energy of the last ion in the buncher. This gives

$$\left(1 - \frac{t_1}{T_0}\right) = \sqrt{\frac{E_0}{E_0 + \Delta E}}$$

or

$$\Delta E = \left[E_0 \quad \frac{1}{\left(1 - t/T_0\right)^2} - 1 \right]. \tag{34}$$

A suitable waveform, given by Equation 34 would, therefore, bunch a group of ions passing the acceleration gap. The foregoing assumes a negligible gap transit time.

For mathematical simplicity the effects of a drift tube will be considered before those of an accelerating tube.

Now place a drift tube of constant potential V_D after the buncher. The particle energy is thus given by E_D for $t = 0$. It will be assumed that the majority of the bunching occurs in the buncher tube so the time spread of the beam at B is small. It is first assumed that the particles reach the gap B when $\Delta E = 0$. In ℓ_1 the particle energy is given by $E_o + \Delta E$, and in ℓ_2 it is given by $(E_o + \Delta E) + (E_D - E_o) = E_D + \Delta E$. The first particle reaches the end of ℓ_2 in time

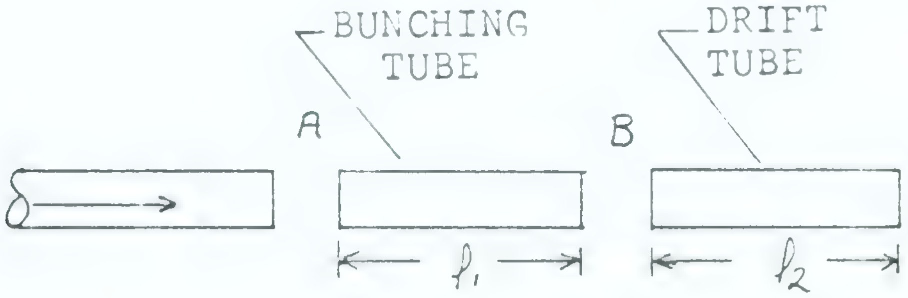

Figure 15. Bunching and Drift Tube System

$$T_0 = T_{01} + T_{02} = \frac{N \ell_1}{\sqrt{E_0}} + \frac{N \ell_2}{\sqrt{E_D}} \quad ; N = \sqrt{m/2} \,. \tag{35}$$

Thus for bunching we have following the previous example

$$\left(1 - \frac{t_1}{T_0}\right) = \frac{T_{01}}{T_0}\sqrt{\frac{E_0}{E_0 + \Delta E}} + \frac{T_{02}}{T_0}\sqrt{\frac{E_D}{E_D + \Delta E}} \,. \tag{36}$$

For case 2 we assume the bunch reaches the gap B at $\Delta E = \Delta E_{max}$. In ℓ_1 the energy is given by $E_o + \Delta E$, and in ℓ_2 by $E_f + \Delta E - \Delta E_{max}$ or $E_D^* + \Delta E$. Now $T_o^* = T_{o1} + T_{o2}^*$ and

$$\left(1 - \frac{t_1}{T_o^*}\right) = \frac{T_{o1}}{T_o^*}\sqrt{\frac{E_o}{E_o+\Delta E}} + \frac{T_{o2}^*}{T_o^*}\sqrt{\frac{E_D^*}{E_D^*+\Delta E}} . \tag{37}$$

To solve for t it is necessary to know ΔE and ΔE_{max}. Further drift tube sections just add additional terms to Equation 37.

Next, an accelerator tube will be placed between the buncher and drift tubes. The end energies are designated as E_{fo} and E_f. The average velocity is given by

$$\bar{v} = v_o + \tfrac{1}{2} a t = v_o + \tfrac{1}{2} a \frac{l_a}{\bar{v}} . \tag{38}$$

Therefore,

$$\bar{v} = \frac{v_o}{2} + \frac{1}{2}\; v_o^2 + 2a l_a \quad = \frac{v_o}{2} + \frac{v_f}{2} . \tag{39}$$

Let $E_a = \frac{1}{2} m \bar{v}^2$. Equation 39 becomes

$$E_a = \frac{1}{4}\left\{ E_{f_o} + E_f + 2\sqrt{E_{f_o}}\,\sqrt{E_f} \right\} . \tag{40}$$

It follows that

$$(T_o - t_1) \propto \frac{\sqrt{m/2}\; l_a}{\sqrt{E_a + \Delta E_a}} \tag{41}$$

where

$$E_a + \Delta E_a = \frac{1}{4}\left\{E_{f_0} + \Delta E + E_f + \Delta E + 2\sqrt{(E_0 + \Delta E)(E_f + \Delta E)}\right\}$$

for case 1. Comparing Equations 41 and 40

$$\begin{aligned} \Delta E_a &= \frac{1}{2}\left\{\Delta E + \sqrt{E_0 + \Delta E}\,\sqrt{E_f + \Delta E} - \sqrt{E_f}\,\sqrt{E_0}\right\} \\ &= \frac{1}{2}\left\{\Delta E + \sqrt{E_f}\,\sqrt{E_{f_0}}\,(\mathcal{K} - 1)\right\} \end{aligned} \tag{42}$$

where

$$\mathcal{K} = \left\{\left(1 + \frac{\Delta E}{E_{f_0}}\right)\left(1 + \frac{\Delta E}{E_f}\right)\right\}^{\frac{1}{2}}.$$

Rearranging Equation 41

$$\left(1 - \frac{t_1}{T_0}\right) = \sqrt{\frac{E_a}{E_a + \Delta E_a}} \; . \tag{43}$$

The bunching criterion for the system of buncher, accelerator, and drift tubes is

$$\left(1 - \frac{t_1}{T_0}\right) = \frac{T_{01}}{T_0}\sqrt{\frac{E_0}{E_0 + \Delta E}} + \frac{T_{02}}{T_0}\sqrt{\frac{E_a}{E_a + \Delta E_a}} + \frac{T_{03}}{T_0}\sqrt{\frac{E_D}{E_D + \Delta E}} \; . \tag{44}$$

Similarly for case 2

$$\left(1 - \frac{t_1}{T_0^*}\right) = \frac{T_{01}}{T_0^*}\sqrt{\frac{E_0}{E_0 + \Delta E}} + \frac{T_{02}^*}{T_0^*}\sqrt{\frac{E_a^*}{E_a^* + \Delta E_a^*}} + \frac{T_{03}^*}{T_0^*}\sqrt{\frac{E_D^*}{E_D^* + \Delta E}} \; . \tag{45}$$

FIGURE 16: APPROXIMATIONS TO THE PERFECT BUNCHING WAVE FORM

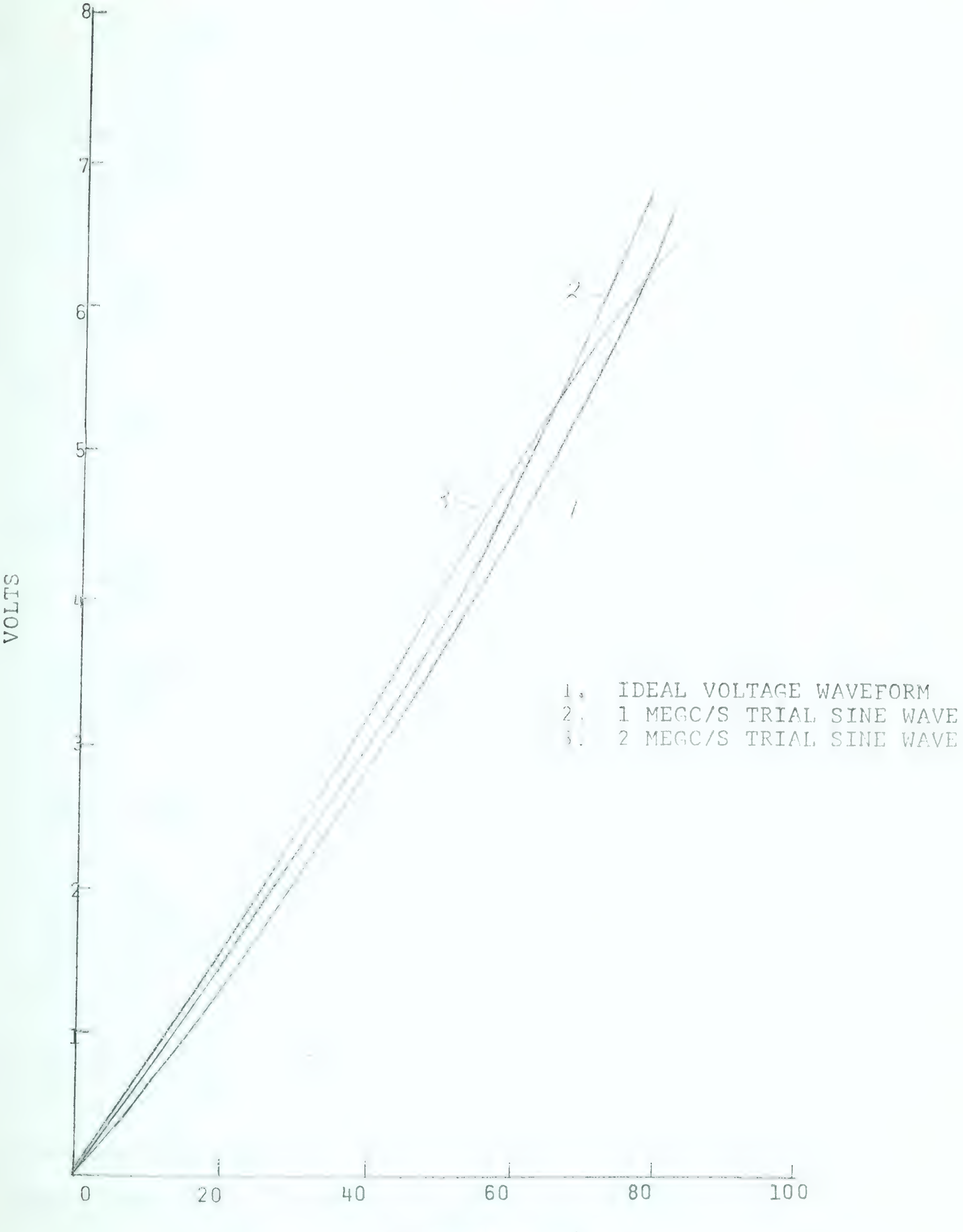

Figure 16 shows that the ideal bunching voltage can be imitated by a portion of a sinusoidal wave. Curve 1 is the idealised curve for a single buncher tube of length 60 cm. with E_o = 15 kev, and having T_o = 500 nanoseconds. The equation is

$$\Delta E = E_o\left\{\frac{1}{(1-t/T_o)^2} - 1\right\}$$

or

$$\Delta E = (15)10^3\left\{\frac{1}{\left(1-\frac{t}{(500)10^{-9}}\right)^2} - 1\right\}.$$

Curve 2 is a plot of the equation

$$\frac{\Delta E}{E_o} = 1.129 - 1.296\cos\left\{(180t/T_o)^{\circ} + 29^{\circ}24'\right\},$$

the equation used by Delenay. It is seen that the modulating frequency is $f = 180/(T_o/2) = 1/(500/2) \times 10^9 = 10^6$ cycles per second. The period of this modulation is 1000 nanoseconds. Curve 2 extends for only 30° of the modulating voltage. It is a good fit in this region but the peak voltage is 38 kv, a difficult voltage to achieve. The bunching factor is greater than 20 for this voltage. The bunching factor represents the ratio of the length of the beam burst before bunching as compared to the length after bunching. It may be defined in terms of the beam pulse durations, i.e. the pre-bunching pulse duration divided by the post-bunching pulse duration. Curve 3 is a plot of the curve

$$\frac{\Delta E}{E_o} = 0.433\left\{\sin\left(\frac{360t}{T}\right)^{\circ} + 0.5\right\}.$$

It is seen that this curve does not fit curve 1 as well. It has a bunching factor of 17. However, as the modulating frequency is 2 mc, the curve extends over 60° and the maximum voltage is 13 kv, a much easier voltage to achieve that the 38 kv of curve 2.

D. Mobley Magnet Buncher

R. C. Mobley (Mo 55) devised the following system for bunching a beam at a target, without introducing an energy spread in the pulse.

Let the beam width be H. For the extreme particles of the beam to arrive at the target simultaneously, it is seen that the inside particle sweep time t^* along ce (Figure 17) must equal the difference in transit times from ce to df of the two particles.

So $t^* = ce/v^*$ and $t^* = (ck + d)/v$

and $v^* = (ce/(ck + d))v$

where v^* = sweep velocity,

and v = mean ion beam velocity

To calculate the pulse length at the target consider the triangle formed by the beam as it initiates its sweep.

$$H/D = (ce)/(ck)$$

by similar triangles.

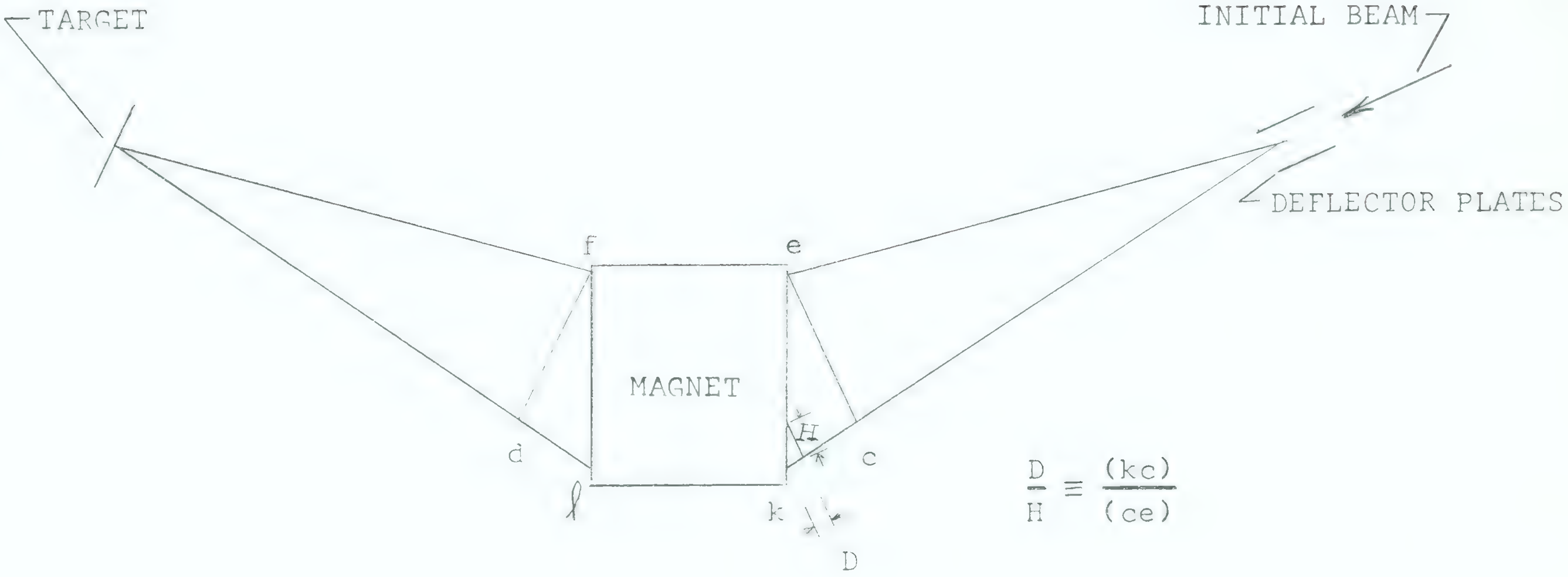

$$\frac{D}{H} \equiv \frac{(kc)}{(ce)}$$

FIGURE 17. MOBLEY COMPRESSION MAGNET

The outer particle takes time

$$(ck + k\ell + \ell d)/v$$

while the inner one takes

$$((ck-D) + k\ell + (\ell d - D))/v .$$

Subtracting one finds

$$\text{time difference} = 2D/v = 2H(ck)/(ce)/v = H/v^{*}.$$

That is, the time spread depends on the width of the beam and inversely on the sweep time.

Advantages of this system are: (1) it reduces the problem of space charge, (2) it does not add appreciably to the energy spread of the beam.

Disadvantages of this system are: (1) it is very expensive, (2) it is very bulky, and (3) for a change in the ion energy a change in the sweep time and a similar change in the magnetic field intensity are required.

CHAPTER III. APPARATUS

A. Introduction

The aim of this work is to construct a preacceleration system which produces an ion beam, consisting of 10 nanosecond pulses which have an instantaneous current greater than the 500 μ amps obtainable with the present pulsing system used in the 5.5 Mev Van de Graaff accelerator. This is to be accomplished by first pulsing the ion source probe thus producing a beam burst lasting longer than 10 nanoseconds and secondly by reducing the length of this beam burst to 10 nanoseconds using a klystron buncher. This system will replace the present preacceleration beam chopping system in the 5.5 Mev Van de Graaff. The 10 nanosecond accelerated pulses from the Van de Graaff are further compressed to 1 nanosecond duration by a Mobley magnet system.

To study the effects of pulsing the probe, and beam bunching, it was necessary to construct a small accelerator. The accelerator consists of the ion source, beam buncher, accelerator tube, momentum filter, drift tube and target.

The source bottle and focus system are those employed in the 2 Mev Van de Graaff accelerator, produced by High

Voltage Engineering. Ion stripping is accomplished by an r.f. oscillator operating at 84 megc/sec. The beam buncher, a 1" diameter cylinder 6" long, is placed between the ion source and focussing electrode. Two accelerator sections were obtained by cutting a standard proton acceleration tube, from the 2.0 Mev Van de Graaff, in half; the high voltage end with injector, etc. is used for the proton accelerator tube, while the low energy end is used as the accelerator tube in the indirect detection system to be explained later. A variflux permanent magnet, placed directly after the proton accelerator tube, is used to separate the mass 2 hydrogen beam coming from the ion source and other ions formed by collisions within the system from the main proton beam. Beam defining slits were used after the magnet to prevent the H_2^+ and any other heavy ions in the system from continuing down the drift tube. A positive potential of 200 volts was placed on these slits to prevent secondary electrons from reaching the detection system and producing a background comparable in magnitude to the signal. The negative H.T., for the accelerator, is produced using a SAMES 150 kv, 2 milliamp supply. Figure 18 shows the relative position of the various parts of the accelerator.

Before pulsing experiments were undertaken the optimum

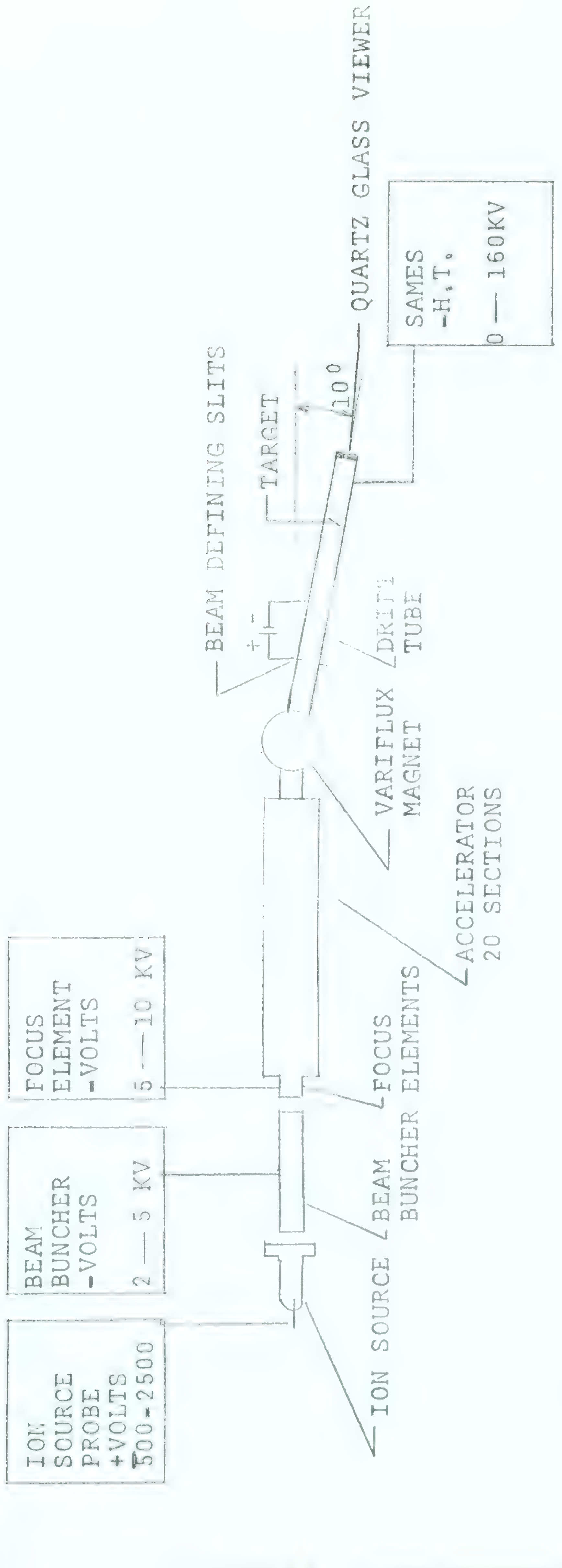

FIGURE 18. ACCELERATOR SECTION

operating conditions for a D.C. ion beam were determined. The total current coming from the ion source was measured as a function of various system parameters.

The methods used to make the above measurements indicate a direct current or the mean current of a pulsed beam. It was necessary therefore to devise alternate methods to detect the shape of the beam pulses. An indirect method (electron detection system) is used for pulsed beam detection. A small tungsten wire is placed in the path of the main proton beam. Some of the protons collide with this wire producing secondary electrons, while the majority of the protons continue on to the target. A fraction of the secondary electrons is attracted into a side tube and accelerated to ground potential where it is detected. Figure 19 is a block diagram indicating the relative positions of the accelerator and electron detection systems.

The use of two accelerating sections permits having the beam detecting equipment and the ion source at ground potential, rather than at the negative H.T. It is easier to work with this equipment when it is at ground potential. Most of the problems encountered by P. Riley (Ri 62) in his previous work in this laboratory are overcome. He used a single accelerating tube so his detection equipment was

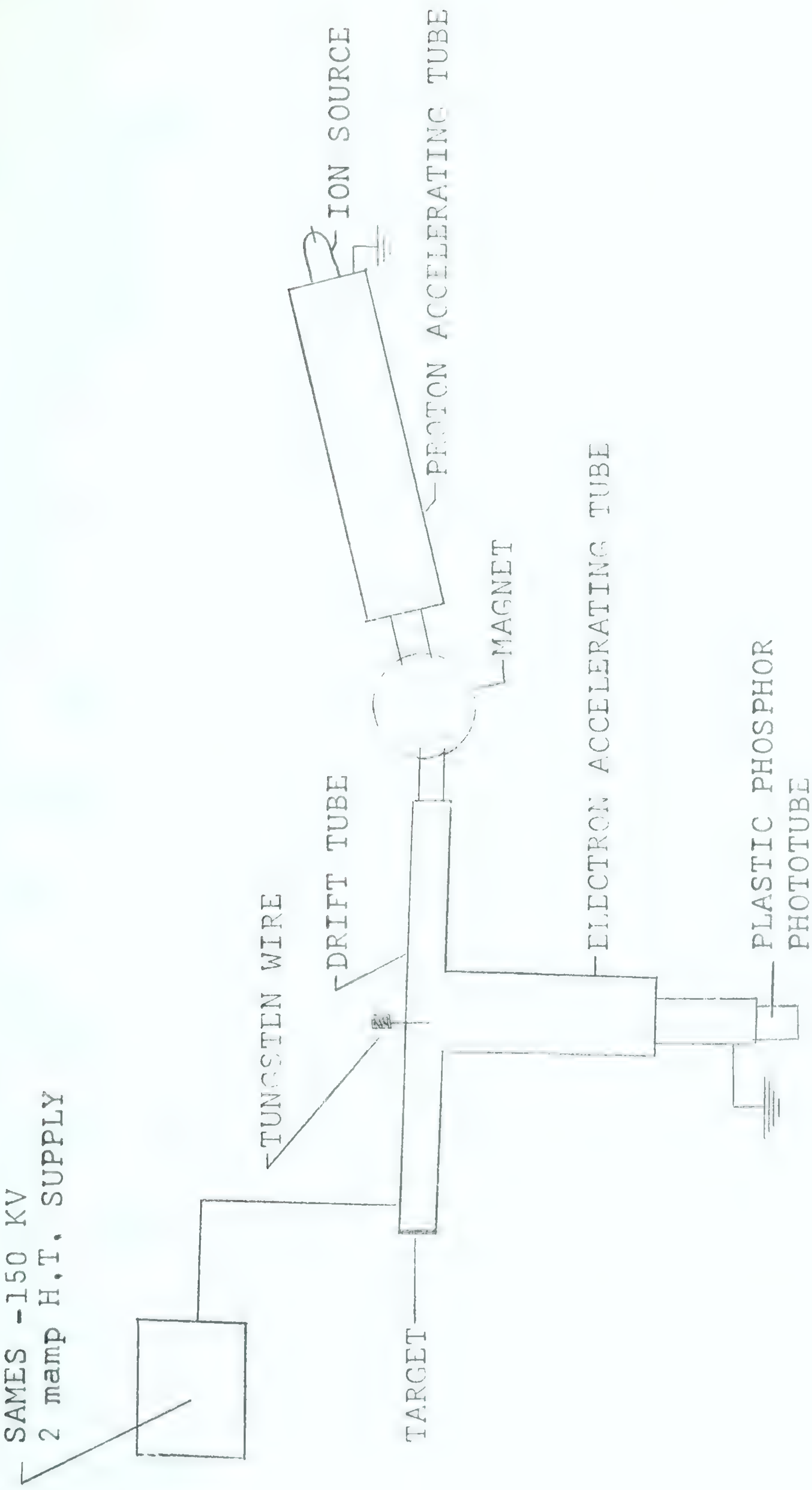

FIGURE 19. BLOCK DIAGRAM OF APPARATUS

at a high potential His main problems were electrical breakdown and a background due to the ion source being in sight of the detector.

To dry the air around the accelerating tubes, permitting the use of higher potentials before breakdown, the complete accelerating system is enclosed in a lucite box. Lucite is used due to its transparency, high surface resistance, and toughness. Silica gel is the drying agent. The frame for the lucite structure is 2-3/4" aluminium I beam; 1/2" steel bolts are used to level the structure.

B. Pulsed Accelerator

The beam bunch production is to be carried out by first pulsing the ion source at approximately 5 megc/sec. followed by Klystron bunching of the beam burst from the ion source.

R.F. Circuitry

1. Beam Buncher

Figure 20 is the circuit diagram for the beam buncher amplifier. The beam buncher voltage, a 2.5 megc/sec. sine wave, is derived using a Textronic variable frequency sine wave generator. This signal is fed into a single tube phase inverter through a push-pull tuned plate amplifier into two Eimac 4 x 150 A's in parallel. They deliver up to 6 amps circulating current, or 6,780 volts rms from a tuned secondary.

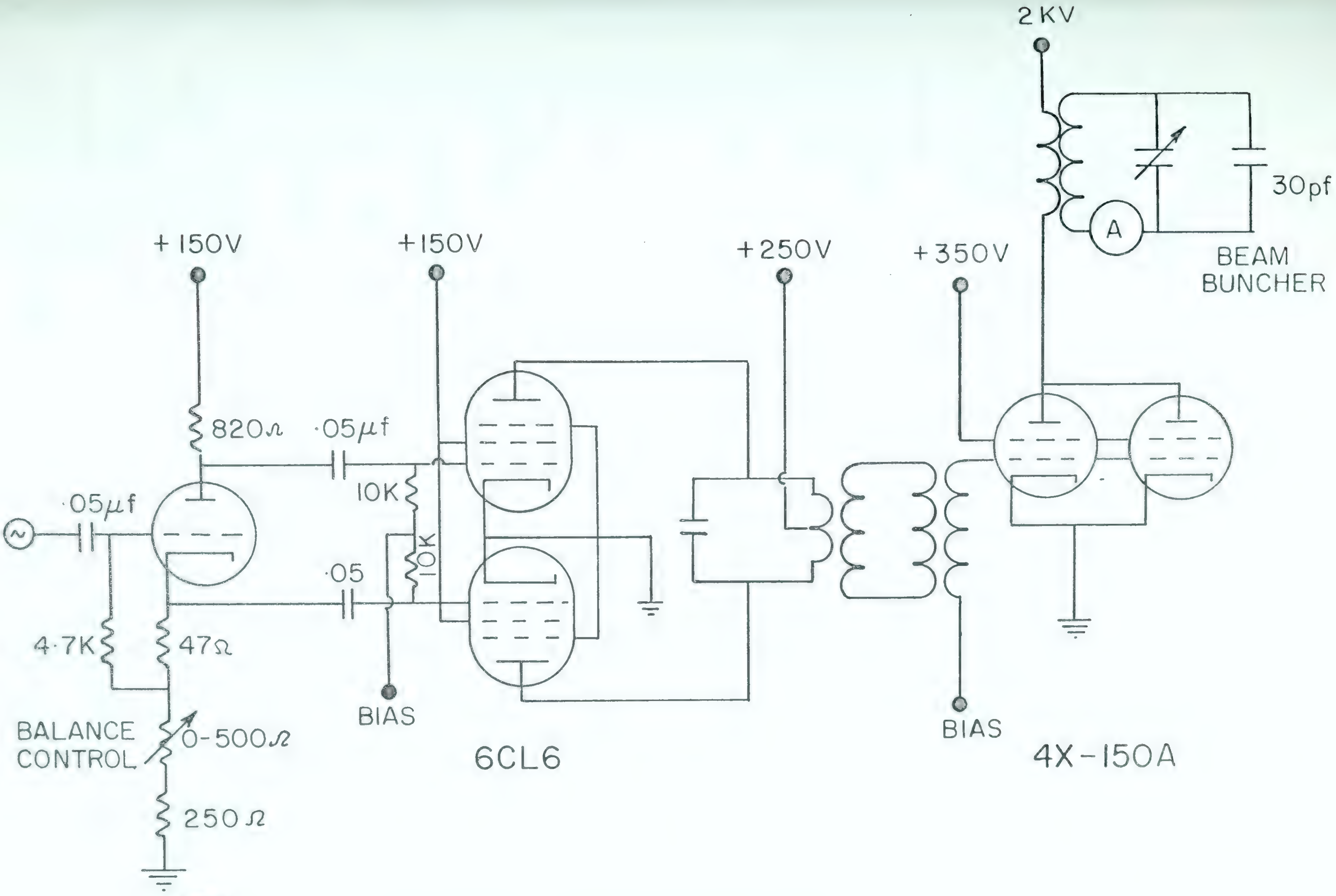

FIGURE 20. BEAM BUNCHER CIRCUIT

2. Probe

Figure 21 shows the probe amplifier. The probe voltage is also derived from the Textronic sine wave generator. The signal is fed through a cathode follower into a $0 \to \pi$ phase shifter. The phase shifter controls the entrance phase of the beam entering the klystron buncher. The shifted voltage is taken off a differential amplifier into two 6CL6's in push-pull, with a tuned plate circuit. These tubes in turn drive an Eimac 4-125A with a tuned secondary. This last stage is operated as a frequency doubler, producing pulses corresponding to 5 megc/sec in the accelerator, with a repetition period of 400 nanoseconds, as the buncher working at 2.5 megcycles/sec. only bunches every second pulse, spreading out the alternate ones (See Chapter 2,C 1)

C. Methods of Detection

1. Direct Detection of Proton Beam

(a) Measurement of Total Current From Ion Source

Quantitative measurements of the proton beam leaving the ion source were made using the beam buncher and focus elements as a Faraday cup. This was accomplished by connecting the high voltage end of the accelerator tube to the ion source probe. When the probe is at a positive

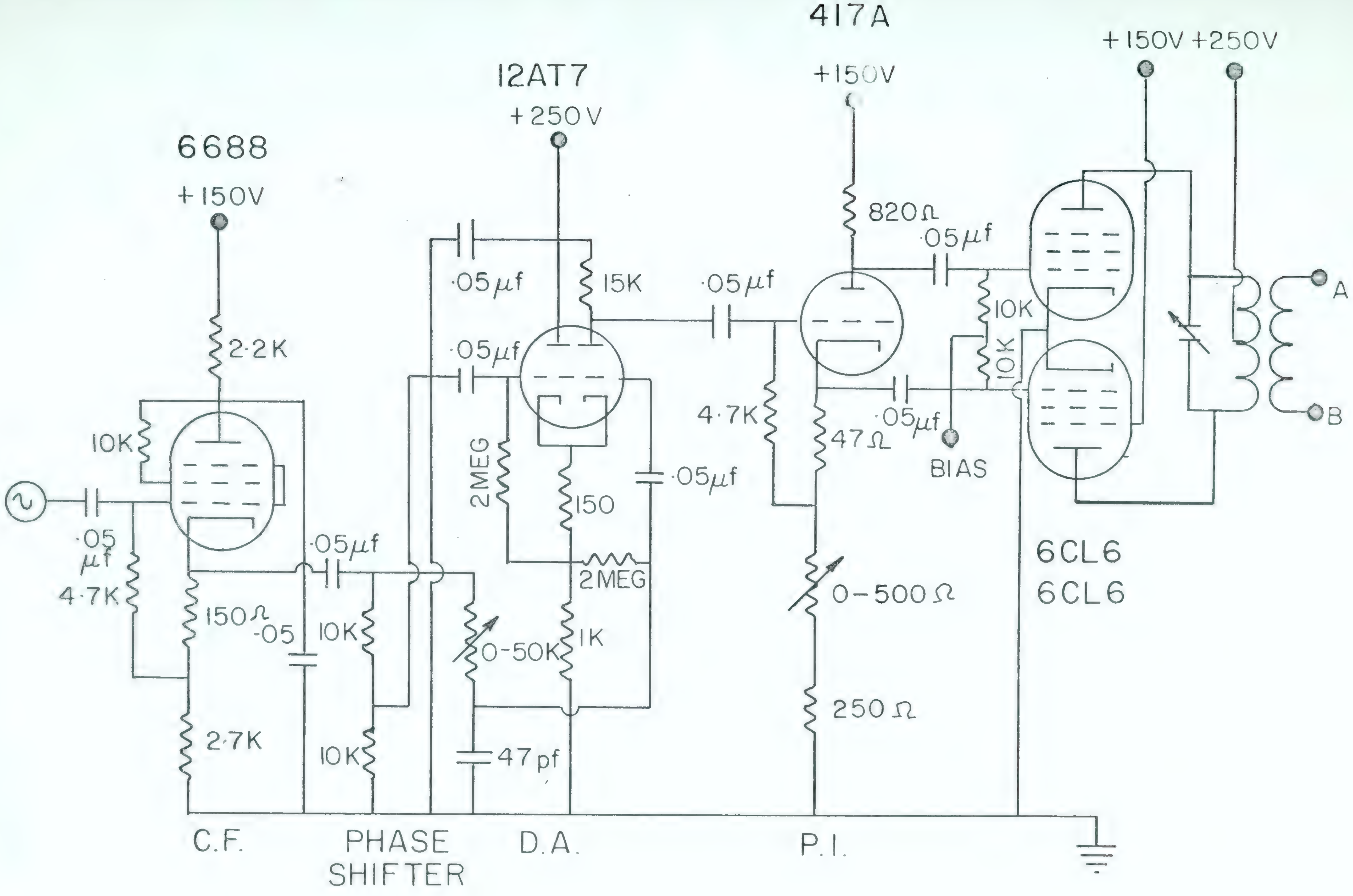

FIGURE 31 PROBE CIRCUIT

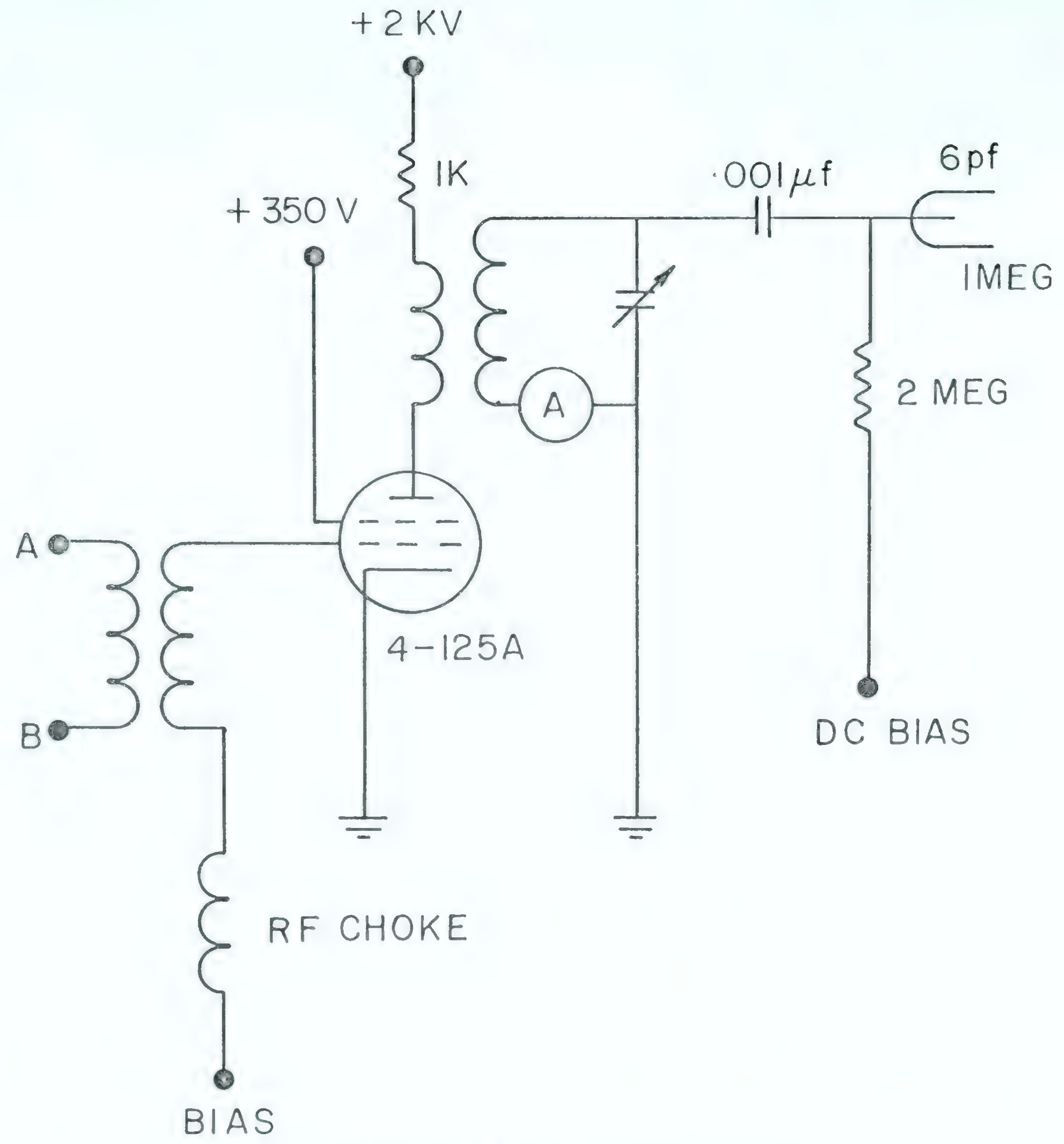

FIGURE 21. PROBE CIRCUIT

potential the ions are forced out, through the beam buncher and focus elements into the accelerator tube. Here the ions see a positive potential, similar to that of the probe, and reverse their direction of flight. The ions finally come to rest on the focus or beam buncher elements. This detection system may be used to measure a direct current beam or to give a mean value of a pulsed beam. An alternate detection system is needed to detect the profile of a pulsed beam.

(b) Measurement of the Accelerated Ion Beam

An absolute measurement of the accelerated proton beam is made by intercepting the complete beam in the drift tube section. The intercepting target is movable, so can be positioned to intercept a portion of the ion beam or to allow the ion beam to continue down the drift tube unperturbed. This detection method is used to measure direct current or the mean current of a pulsed beam.

(c) Visual Inspection for Focussing

The proton beam is permitted to impinge upon a quartz glass blanking plate at the end of the drift tube section, permitting a visual inspection of the beam diameter.

2. Indirect Detection of Proton Beam

This detection method is based on the detection of secondary electrons produced by the main proton beam upon collision with a small tungsten wire. This wire may be rotated partially out of the proton beam, decreasing the number of secondary electrons produced. Figure 22 is a line diagram of this detection system. The electrons form a plasma from which some of the electrons are attracted into the detection system, while others recombine with protons in the accelerator drift tube.

Figure 22 is a schematic of this indirect detector system. The first electrode attracts the electrons into the detection system. It has a positive potential with respect to the accelerator drift tube. The target can be put at a negative potential with respect to the accelerator drift tube to force the secondary electrons away. The voltage on the second and third electrodes, which serve to focus the electron beam, may be varied independently. Increasing the potential on the third electrode stiffens the electron beam, pulling the focal point nearer to the lens system. An increased voltage ratio of electrode 2 to electrode 3 with respect to H.T. decreases the focal length.

Focus indicating rings are placed in the drift tube

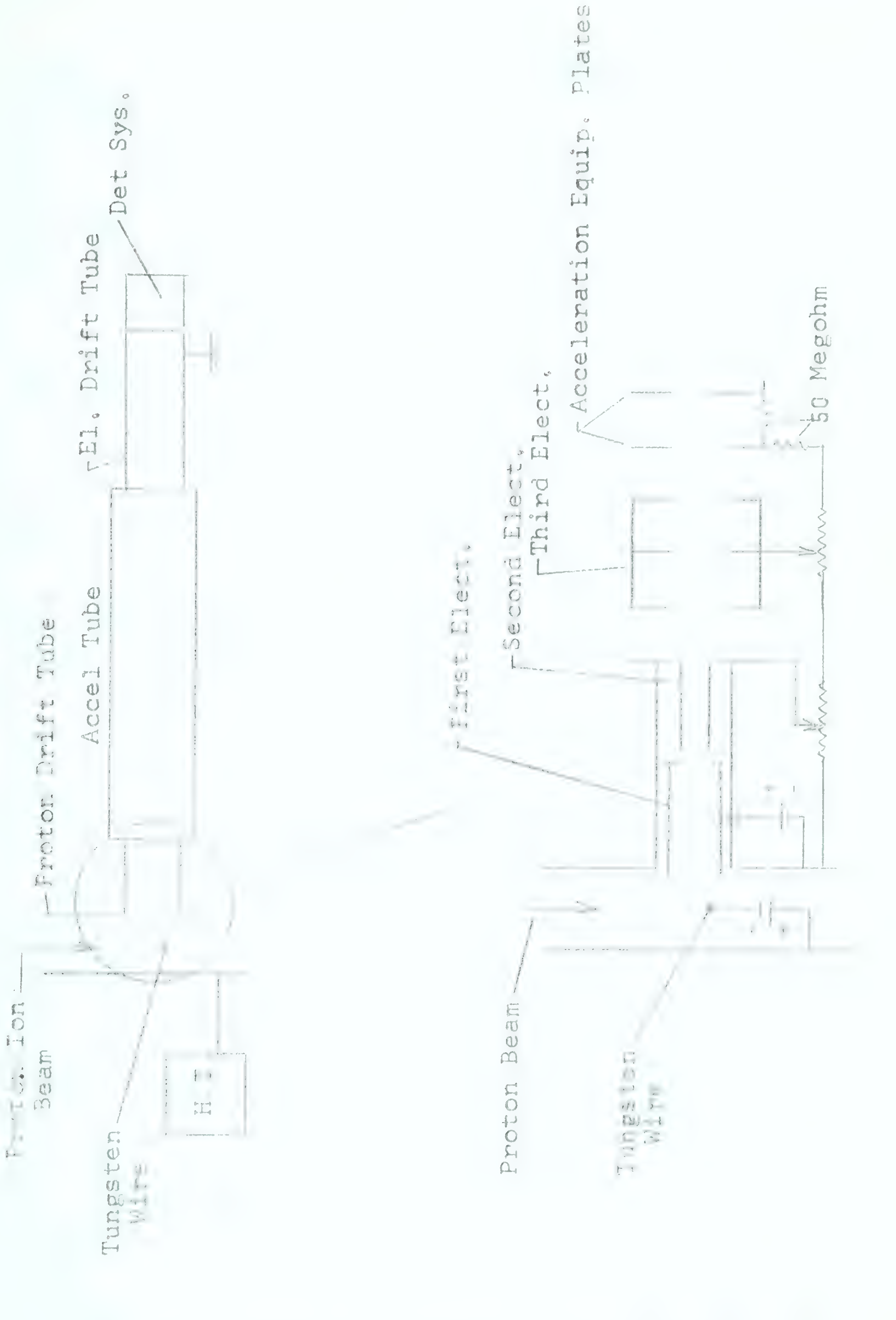

FIGURE 22. Indirect Detection System

sections. The one closest to the ion source has a 1-1/4" diameter hole while the second has a 1 " diameter hole. Microammeters are connected to each of these rings. A Faraday cup (1-1/4" diameter) and electrometer are used to measure the electron current reaching the end of the drift tube section.

The voltages on the two focussing electrodes are varied until minimum current is indicated on the focus indicating rings and maximum current on the electrometer. A voltage ratio of 8 or 9 to 1 (third to second electrodes) produces this optimum condition.

As shown in Figure 22 all the column resistors are of the same value, 50 megohms.

It has been suggested that this be changed. Smaller valued resistors should be placed at the high voltage end of the accelerator tube. The column resistors would then increase in magnitude to the low voltage end of the tube such that the average column resistor value is again 100 megohms. This resistor variation sets up smaller voltage differences across the accelerator equipotential plates at the high energy end leading to a smoother focussing action. This effect on the voltage gradient also tends to increase the flight time of the electrons in the accelerating tube. The focal point of the beam will move closer to the high voltage end of the accelerator, for the same focussing voltages used with the 50 megohm column resistors.

Various methods are used to detect this electron beam.

(a) Faraday Cup at End of Electron Accelerator Tube

The first method used is to place a Faraday cup at the end of the accelerating tube. A D.C. beam can be measured using an electrometer on the Faraday cup output. For detection of a pulsed beam the Faraday cup output is fed into a series of Hewlett-Packard wide band amplifiers. No pulses were detected using this system. Further measurements show a peak electron current of approximately 1.4 microamps when the entire proton beam is intercepted leading to a pulse height of about 0.28 millivolts before amplification. As the basic noise level of the Hewlett Packard amplifiers is approximately 1 mv, these pulses cannot be detected. It would be necessary to increase the average current to at least 10 microamps to detect electron pulses using this method.

An attempt to increase this current was made by placing a wire in front of the Faraday cup. It was hoped this wire, with a positive potential on it, would pull electrons from the outer sections of the drift tube into the central region where they would be detected by the Faraday cup. No noticeable increase in current was found.

This detection system could be further improved by

employing magnetic focussing in the drift tube section. Simple experiments show that the beam intensity can be increased by a factor of 10 using magnetic focussing. An angular magnet should be placed around the drift tube after the accelerator. Its magnetic field would pinch the electron beam onto the tube axis. The magnetic field may be varied, through the current, as well as the magnet's distance from the Faraday cup.

The preacceleration electron focussing system should also be improved.

(b) Photomultiplier at End of Electron Accelerator Tube

Another direct method of detecting a pulsed electron beam consists of placing a R.C.A. 6342 photomultiplier with a plastic phosphor on its photocathode directly on the end of the accelerator tube. A Tectronix 545 oscilloscope was used to display the photomultiplier output. It was found that the electron beam being detected was too intense for the photomultiplier to handle. Measurements with a Faraday cup and electrometer showed an average electron current greater than 10^7 amps or 10^{12} electrons per second. It is desirable to decrease the detected value to 10^9 electrons per second. This reduction may be carried out by mounting a small plastic phosphor on a cone of light pipe, leading to the photomultiplier. The

small plastic phosphor would be placed in the centre of the drift tube section, after the electron accelerator tube, with a collimator preventing the electron beam from striking the light pipe. X-rays produced at the collimator are not detected due to the small size of the phosphor.

(c) Photomultiplier in Side Tube

A second indirect method for detection of the pulsed proton beam is used, again based on the production of secondary electrons. This time secondary electrons are produced by the main electron beam colliding with a tungsten wire. Two cup shaped electrodes pull electrons into a side tube where they are detected by an R.C.A. 6342 photomultiplier which has the photocathode cut off. Having no photocathode, or plastic phosphor, thus doing away with the processes of changing electrons to photons, to electrons, decreases the detection time dispersion. Here again the detected beam intensity is too great, burning out the photomultiplier. This photomultiplier is replaced by another R.C.A. 6342 photomultiplier with a small plastic phosphor attached to the photocathode. The gamma ray detection efficiency is reduced greatly compared to the previous plastic phosphor-photomultiplier systems used due to the small size of the plastic phosphor.

This detection method permits the detection of individual pulses due to the pulsing of the accelerator ion source probe by an r.f. signal.

D. System Characteristics

1. Accelerator Characteristics

(a) Extractor Characteristics

The following table shows the effects of the hydrogen gas concentration in the ion source bottle on the proton beam. The changes in the proton beam are measured using detection system 1(b). Hydrogen concentration is related to the paladium leak heater current.

The table lists various heater currents and the corresponding maximum proton target current with the probe voltages at which these maximums occur. The proton current decreases when the ion source hydrogen concentration becomes excessive (> 250 ma) as the ion stripping oscillator lowers in efficiency. When the hydrogen concentration is low (< 150 ma), the supply of hydrogen ions is lowered leading to a low proton beam current. The optimum leak heater current seems to be in the 150 to 160 ma range.

Leak Heater Current (ma)	Detector Current (μa)	Probe (volts)
200	14	1500
190	18	1500
180	26	1800
170	35	1800
160	50	1800
150	50+	1700-2000
140	34	1500-2000
130	16	1500-2000

System Parameters are:

Ion r.f. Stripper @100 ma plate, 1 ma grid.
Beam Buncher 4.8 kv
Focus Electrode 9.8 kv

(b) Probe Characteristics

Figure 23(1) shows the variation in total proton current from ion source with probe voltage. The proton current increases fairly linearly with the probe voltage for probe voltages between 500 and 1500 volts. A maximum proton current is reached at 2000 volts. For probe voltages above 2000 volts the proton current decreases with increasing probe voltage. This is a consequence of the physical construction of the ion source in that at these high voltages

FIGURE 23. PROTON BEAM CHARACTERISTICS

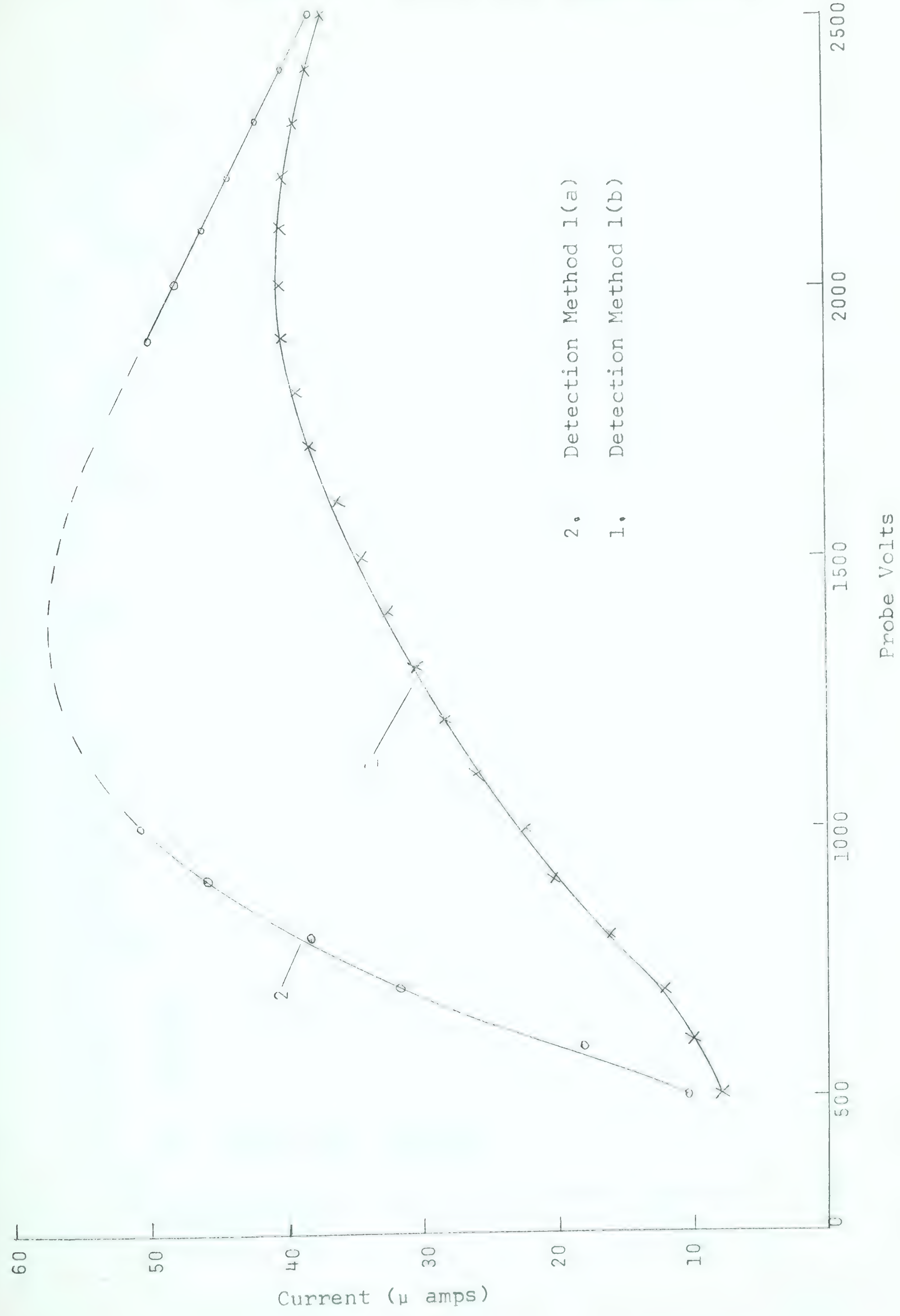

the tendency of the probe to force ions to the outer walls of the ion source, rather than towards the source exit, becomes dominant.

System parameter settings are:

Leak current 160 ma
Ion oscillator 112 ma plate, 3.89 ma grid

Its settings are very critical to the operation of the ion source.

The oscillator should be run with minimum grid current for maximum ion beam current.

B.B. & Focus - used as Faraday cup.

Figure 23 (2) is the accelerated proton beam measured with a 130 volts potential, negative with respect to the drift tube on the beam intercepting target. The current reading is then the proton current plus the secondary electron current. As the meter only goes up to 50 μ amps the section of curve 2 above this value is arrived at from the trends of the current curve at low and high probe voltages.

System parameters here are:

Leak current 160 ma.
Ion oscillator 160 ma.
B.B. 4.1 kv.
Focus 10.4 kv.

(c) Proton Beam Focussing

The accelerator has the same focussing system as in the

FIGURE 24. ELECTRON CURRENT VS. PROBE VOLTS

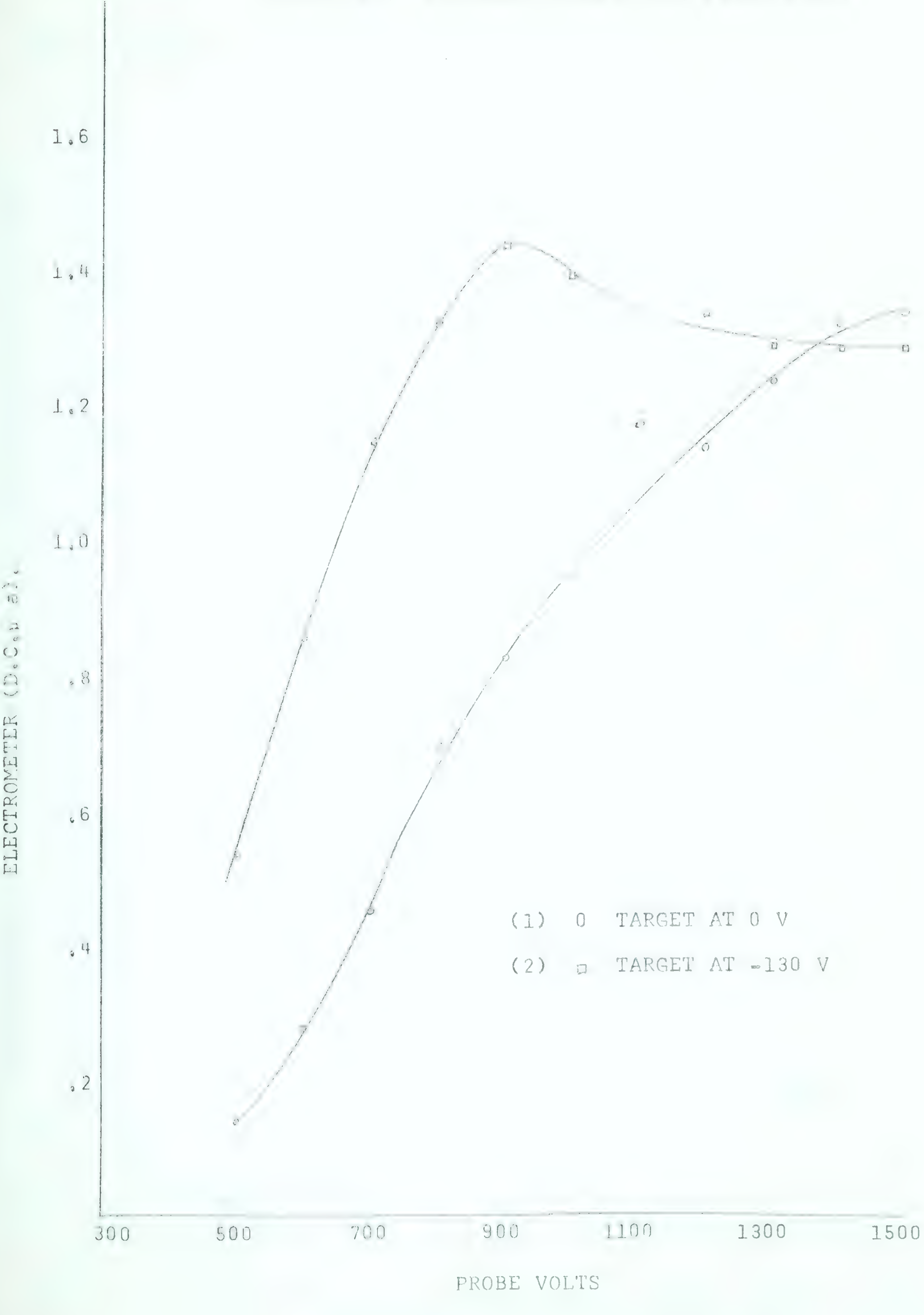

FIGURE 25.R.M.S. ELECTRON CURRENT VS. PROBE r.f. VOLTS

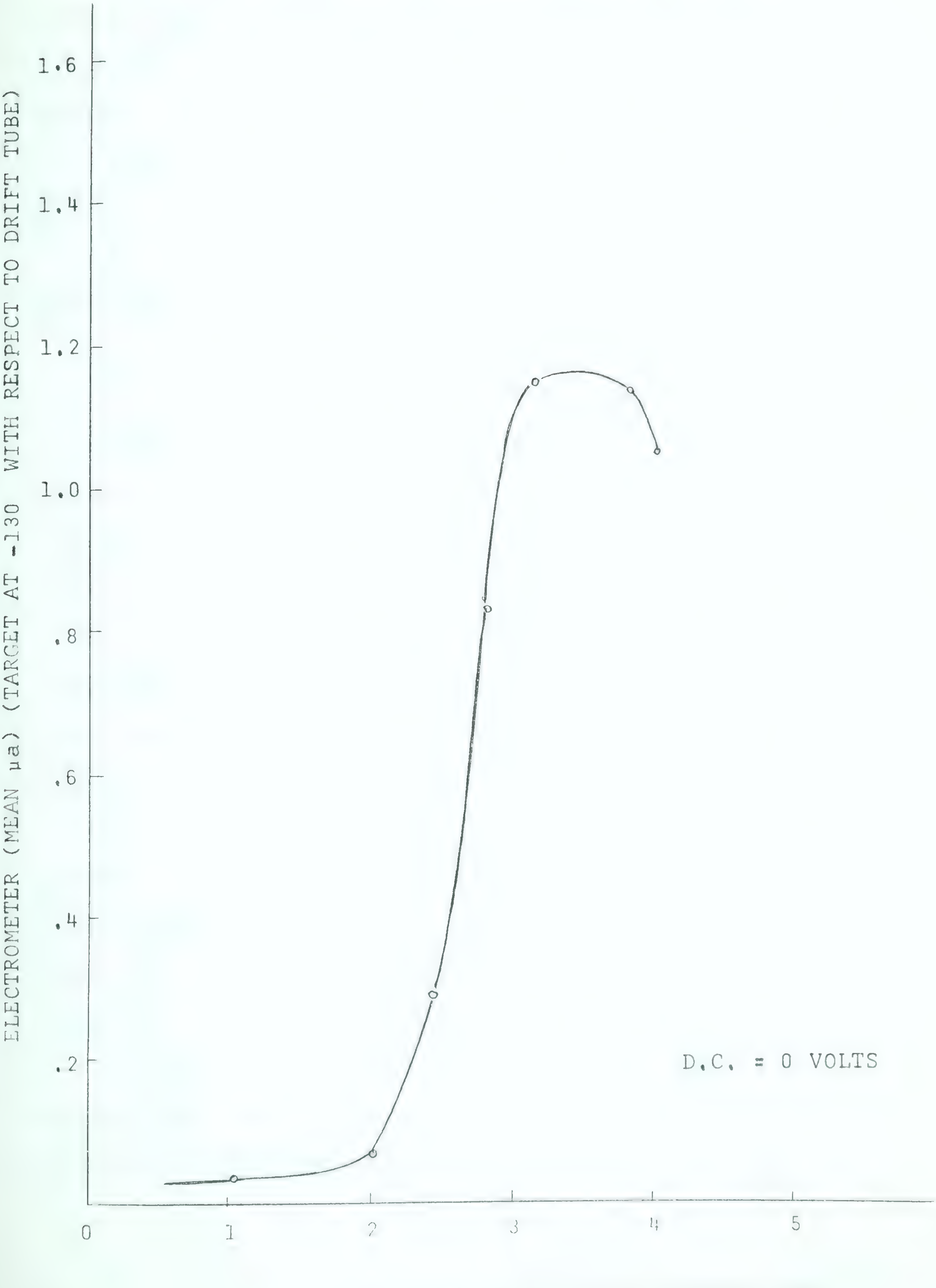

2.0 Mev Van de Graaff with the exception of an additional bunching tube between the ion source and the focussing element.

With the SAMES H.T. at -120 kv a focussing voltage of 9.7 kv to 10.0 kv along with a beam buncher voltage of -4.4 kv produces a proton beam at the target end of the drift tube with a cross-section of approximately 1/10".

2. Electron Beam Characteristics

Figure 24 shows the effect of having a negative voltage relative to drift tube on the tungsten wire in the proton drift tube. This negative potential tends to drive away the secondary electrons, diminishing the chance of an electron and proton recombining. The current indicated on the microammeter is doubled when the target has a negative potential. This fact is born out by Figure 19 up to a probe voltage of 900 volts. Above this voltage the measured electron current lowers. This decrease in measured current may be attributed to a recombination of electrons with the more intense proton beam, thus a lowering of the number of electrons being pulled into the detection system.

Figure 25 shows the r.f. probe voltage and corresponding electrometer readings from detection method 2(a). It is seen that no appreciable ion beam is formed for an

r.f. circulating current below 2 amps. on the probe. At 3 amps. the ion beam current has increased to its maximum. For an r.f. circulating current greater than 3.75 amps. the ion beam current tends to decrease as it does for a high d.c. probe voltage.

The pulse shape expected without bunching is shown in Figure 26. It has a half-width of 36 nanoseconds. The shape of the pulse was determined using the D.C. electron beam charasteristics of Figure 19(b), assuming the ion source can follow the 5 megc/sec. sine wave voltage on the probe.

FIGURE ELECTRON CURRENT VS. TIME (PULSE TIME PROFILE)

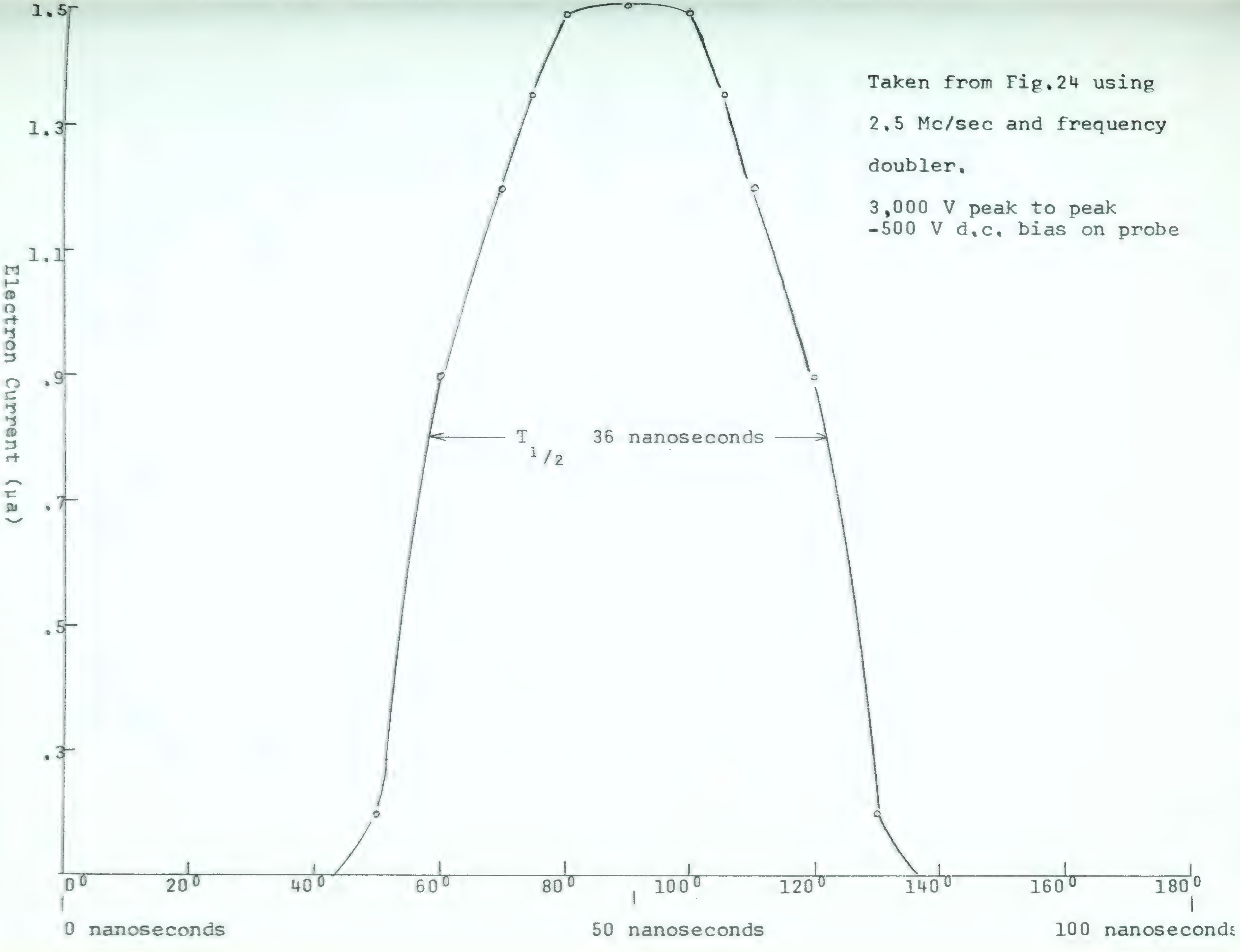

Taken from Fig.24 using

2.5 Mc/sec and frequency

doubler.

3,000 V peak to peak
-500 V d.c. bias on probe

CHAPTER IV

A. Results

The 5.5 Mev Van de Graaff accelerator at the University of Alberta presently employs a preacceleration beam chopper which produces 500 μ amp beam bunches of 10 nanoseconds duration.

The aim of the present work is to develope a top terminal pulsing device which produces higher intensity 10 nanosecond pulses, by first pulsing the ion source producing a beam burst longer than 10 nanoseconds, followed by Klystron bunching of this beam to produce the desired 10 nanosecond beam burst.

There were two main problems; the first was to produce a beam pulse of 10 nanoseconds duration, the second was to detect the profile of this pulse. These problems are inherently connected. It is sometimes difficult to say just which system, the accelerator or the detection, is at fault. The direct methods (Section III, C.1) used to detect the positive ion beam are not applicable to a pulsed beam. It is thus necessary to use an indirect method of detection, based on the production of secondary electrons in the proton beam drift tube. These secondary electrons are

accelerated to and detected at ground potential. Direct detection (Section III, C.2 (a) and (b)) of this pulsed electron beam using a Faraday cup failed, as the mean electron current was too small ($\approx 1\ \mu$ amp) to be detected above the basic noise level of the wide band amplifiers used, even with the system running at maximum electron beam output. This was also the case using a plastic phosphor-photomultiplier detection system, as the electron beam saturated the photomultiplier, even when the system was set for minimum electron beam current.

A second indirect method of detection was established, again based on the detection of secondary electrons. Secondary electrons produced by the electron beam colliding with a tungsten wire are detected in a side tube at the grounded end of the electron accelerator tube by a plastic phosphor-photomultiplier system. The electronics of the photomultiplier circuit has a rise time of approximately 20 nanoseconds, permitting the detection of the beam bunch profiles produced to date. Focussing electrodes permit the use of a small plastic phosphor, lowering the gamma ray detection efficiency.

This last detection system induces a band spectrum of bright and fairly dark sectionson a Textronix 545 oscilloscope. The spectrum has the repetition rate of the r.f. voltage on the ion source probe.

B. Conclusions

Experiments to date indicate that the r.f. signal on the ion source probe is modulating the ion beam.

With only an r.f. voltage on the probe (no d.c.) the detection system indicates that the beam is modulated showing a band spectrum. The ion beam current does not seem to cut off during the negative portion of the probe signal. This effect may, in part, be caused by the detection system itself. A significant time spread of the beam bunch may be introduced when the secondary electrons are pulled into the focussing systems. This dispersion effect would tend to spread out the detected beam bunches. The use of higher attractive fields would diminish this time dispersion.

The presence of a negative d.c. voltage on the probe, in addition to the r.f., seems to decrease the over-all intensity of the beam as expected. The main beam bunches do not appear to be of shorter duration. The beam associated pulses, corresponding to a mean pulsed beam current of approximately 10 μ amps, are around 200 millivolts while the r.f. pickup is 10 millivolts and the signal (not associated with the ion beam) from the photomultiplier is approximately 5 millivolts.

Further experimentation with various combinations of r.f. and d.c. probe voltages should lead to the attainment

of better beam bunches. The d.c. voltage would probably be more negative than the 2,500 volts used to date, with a correspondingly larger r.f. voltage. These larger voltages may give an intense beam burst of shorter time duration than is obtainable at present (Figure 25), with lower beam current from the ion source between the main beam bursts. One problem of using higher voltages is whether or not the ion source can stand probe voltages greater than the rated 2,500 volts without breaking down.

APPENDIX

Definition of Symbols

Symbol	Page	Definition
ΔX	25	Displacement off axis of exit beam having zero angular deviation
ℓ_1	27	Length of deflector plates
ℓ_2	27	Distance from deflector plates to beam defining slits
v_0	27	Initial ion beam velocity
T	27	Period of r.f. voltage on deflector plates
V_0	28	Peak r.f. voltage on deflector plates
y_{sc}	28	Displacement of beam off axis at slits
$y(\ell_1)$	28	Displacement of beam off axis at exit end of deflector plates
$\dot{y}(\ell_1)$	28	Transverse ion velocity at exit end of deflector plates
τ_2	28	Transit time of ion from deflector plates to slits
τ_1	29	Transit time of ion through deflector plates
Δy_{sc}	29	Beam width at slits
$\Delta\delta$	29	Acceptance phase interval for beam bunch passed through slits
Δt_0	29	Acceptance time interval for beam bunch passed through slits

Symbol	Page	Definition of Symbols
W.S.	30	Writing speed = $\Delta y_{sc}/\Delta t_0$
S	30	Slits
δ_0	33	Difference from zero voltage phase, of voltage phase upon the particles entrance into plates
δ_1	33	Deflector plate length in radians = $\frac{\omega l_1}{v_0}$
k	33	Lever arm = l_2/l_1
V_{AC0}	32	Maximum r.f. voltage on both deflector plates
V_{DC1}	32	D.C. voltage on first deflector plate
V_{DC2}	32	D.C. voltage on second deflector plate
H	38	Total energy of ion
E	39	Kinetic energy of ion
τ_0	41	$\tau_0 = \tau_1 + \tau_2 = \tau_1(1 + k)$
δ^1	42	$\delta^1 = \delta_1 + \delta_2 = \delta_1(1 + k)$
$_0$	42	Finite beam radius at exit of deflector plates
α	43	Small half angle divergence of beam
T_1	46	Kinetic energy of incident axial ray beyond deflector plates
dE_1	46	Increase in energy of incident axial ray due to deflector plates
$\left.\begin{matrix}a\\b\end{matrix}\right\}$	48	Position coordinates of virtual ion source in deflector plates
V.S.	48	Virtual source
Y_n	50	Displacement of beam off axis with no refractor plates
Y	50	Displacement of beam off axis with refractor plates

Symbol	Page	Definition of Symbols
τ_1	50	Transit time through deflector plates
τ_2, τ_n	50	Transit time through refractor plates
τ_3	50	Transit time from refractor plates to slits
E_0	54	Initial field on beam buncher
T_0	55	Transit time from front of beam buncher to target with zero modulation
ΔE	55	Modulation on beam buncher
E_D	56	Field in drift tube
E_{f_0}	57	Field at low energy end of accelerator
E_f	57	Field at high energy end of accelerator
τ^*	60	Beam sweep time
v^*	60	Beam sweep velocity
v	60	Mean ion beam energy
H	60	Beam width

REFERENCES

Ad 53 Adair, Okazaki, and Walt. *Phys. Rev.*, 89, 1165 (1953).

Al 55 Allen, Ferguson, and Roberts. *Proc. Phys. Soc.*, (London) 68A, 650 (1955).

Ba 40 H. H. Barschall and M. H. Kanner. *Phys. Rev.*, 58, 590 (1940).

Ba 60 R. Batchelor and G. C. Morrison. *Fast Neutron Physics, Part I*, Chapter III.C., Interscience Publishers, Inc. New York (1960).

Bl 56 S. D. Bloom and C. M. Turner. *Bull. Am. Soc.*, Ser.II, 1, 177 (1956).

Br 62 D. A. Bromley. *Nucleonics*, 55 (May, 1962).

Ce 56 CERN Symposium, Vol. II (1956).

Da 61 J. W. T. Dabbs, F. J. Walters, eds. *Semiconductor Nuclear Particle Detectors*, NAS-NRC Publication 871, Nuclear Science Report No. 2 (1961).

De 55 C. Delaney. Atomic Energy Research Establ. (Gt. Brit.) Report NP/R 1666 (1955).

Fe 60 A. T. G. Ferguson. *Fast Neutron Physics, Part I*, Chapter II.A., Interscience Publishers, Inc. New York (1960).

Fo 55 J. L. Fowler and C. H. Johnson. *Phys. Rev.*98, 724 (1955).

Fr 58 J. S. Fraser and J. C. D. Milton. *Nuclear Instr.* 2, 275 (1958).

Gi 50 R. Giles. *Proceedings of the Harwell Conference on Nuclear Physics* (1950).

Gi 53 R. Giles. *Rev. Sci. Instr.* 24, 986 (1953).

Gl 52 D. A. Glaser, Phys. Rev., 87, 665 (1952); 91, 762, (1953); 97, 474 (1955).

Gr 58 R. E. Green and R. E. Bell. Nuclear Instr., 3, 127 (1958).

IRE 61 Solid State Radiation Detectors, IRE Trans. on Nuclear Sci., NS-8 (1961).

Ja 51 D. B. James and P. B. Treacy. Proc. Phys. Soc. (London), A64, 947 (1951).

Jo 56 G. Jones and J. B. Warren. J. Sci. Instr., 33, 429 (1956).

La 60 R. W. Lamphere. Fast Neutron Physics, Part I, Chapter III.E., Interscience Publishers, Inc., New York (1960).

Le 55 Lepri, Mezzette and Stoppini. Rev. Sci. Instr., 28, 936 (1955).

Le 59 H. W. Lefevre and J. T. Russell. Hanford Report HW-49669 (1957). Electronics, Vol. 32, No. 10, 44(1959). Rev. Sci. Instr., 30, 159 (1959).

Mo 52a R. C. Mobley. Phys. Rev., 88, 360 (1952).

Mo 52b N. F. Moody. Electronics Eng., 24, 289 (1952).

Ne 55 G. C. Neilson and D. B. James. Rev. Sci. Instr., 26, 1018 (1955).

Ne 56 Neiler, et al. Bull. Am. Phys. Soc., Ser II, 1, 70 91956).

Ne 60a G. C. Neilson, W. K. Dawson, F. A. Johnson, and J. T. Sample. A Fast Neutron Time-of-Flight Spectrometer with Applications, Suffield Technical Paper No. 176, DRB (1960).

Ne 60b J. H. Neiler and W. M. Good. Fast Neutron Physics, Part I, Chapter IV.A., Interscience Publishers,

Pe 56 G. J. Perlow. Rev. Sci. Instr., 27, 460 (1956).

Re 57 P. E. Remy and K. Winter. J. Phys. Radium, 18, 112A (1957).

Ri 62 J. Riley. Ph.D. Thesis, University of Alberta (1962).

Sn 53 N. Snowden, in O. Frisch, ed. *Progress in Nuclear Physics, Vol. 3, Pergamon, London (1953).*

St 60 W. E. Stephens and H. Staub. *Fast Neutron Physics, Part I*, Chapter II.E., Interscience Publishers, Inc., New York (1960).

Sw 60 C. D. Swatz and George E. Owen. *Fast Neutron Physics, Part I*, Chapter II.B., Interscience Publishers, Inc., New York (1960).

Tu 49 C. M. Turner, *et al.* UCRL, 352 (1949).

Tu 53 P. R. Tunnicliffe. *Phys. Rev.*, 89, 1247 (1953).

Tu 58 C. M. Turner and S. D. Bloom. *Rev. Sci. Instr.*, 29, 480 (1958).

We 56 Weber, Johnstone and Cranberg. *Rev. Sci. Instr.*, 27, 166 (1956).